Dark matter candidates and dark matter searches

G. Bélanger
LAPTH, Univ. de Savoie, CNRS, B.P. 110, F-74941, Annecy-le-Vieux, France

Abstract

These notes are based on lectures given at EPFL Lausanne for the *3eme cycle de la physique en Suisse romande*

Chapitre 1

Evidence for dark matter

The first observations indicating that there was non-luminous matter were made in 1933 by a Swiss astronomer working at Caltech, Fritz Zwicky, that measured mass-to-light ratios in galaxy clusters. Since then numerous observations from the galactic scale to cosmological scale have provided more evidence that most of the matter in the Universe is dark. Here we briefly described some of this evidence.

1.1 Mass-to-light ratio

The mass-to-ligt ratio is the ratio of the mass of an object to its total luminosity. The mass and luminosity are usually measured in terms of solar mass and solar luminosity, hence the mass-to-light ratio of the Sun is 1.

The mean luminosity of galaxies can be computed given a distribution of galaxies with total luminosity L, $\phi(L)$

$$\mathcal{L} = \int L\phi(L)dL \tag{1.1}$$

This quantity is measured to be $\mathcal{L} \approx 2 \pm 0.3 \times 10^8 h_0 L_\odot Mpc^{-3}$. where $L_\odot = 3.8 \times 10^{33}$erg/s is the solar luminosity and $H_0 = 100h_0 km/s/Mpc$ is the Hubble parameter. Defining the critical energy density,

$$\rho_c = \frac{8H^2}{8\pi G_N} = 1.88 \times 10^{-29} h_0^2 \text{gcm}^{-3} \tag{1.2}$$

the critical mass-to-light ratio reads

$$(M/L)_c = \rho_c/\mathcal{L} \approx 1390 M_\odot/L_\odot \tag{1.3}$$

This can be used to determine the cosmological matter density

$$\Omega_m = \frac{\rho}{\rho_c} = \frac{M/L}{(M/L)_c} \tag{1.4}$$

A useful measure of mass is obtained by taking the ratio of the mass of all stars to the luminosity emitted by all stars in a volume of a few hundred parsecs around the Sun. If the typical star near the sun was equal in mass to the Sun, the ratio of total mass to total light would be unity, larger than unity if the typical star was less massive, and smaller than unity for more massive stars. Since the ratio is found to be 2 for nearby stars, there is little necessity for any dark matter other than the dark dwarfs in the Sun neighbourhood. At larger scales, for example that of small group of galaxies $M/L \approx 60-180h_0$ so that the matter density $\Omega_m \approx 0.1$ while on the scale of cluster of galaxies the mass-to-light ratio is even larger $M/L \approx 200 - 500h_0$ thus implying $\Omega_m = 0.3$. The high values inferred for galaxies and clusters of galaxies indicates the existence of considerable amounts of dark matter. An overview of the observational evidence for dark matter will be given below. The hypothesis of dark matter is also supported by theoretical arguments, dark matter is predicted in most inflation models and galaxy formation requires dark matter to account for the growth of density fluctuations.

1.1.1 Rotation curve of spiral galaxies

One of the most convincing evidence for dark matter on the galactic scale results from observations of rotation curves of galaxies, in particular the circular velocities of stars and gas at a distance r from the center. The rotational velocity of clouds of neutral hydrogen as a function of the distance r is measured by observing 21 cm emission lines and combining this with optical surface photometry. Typical rotation curves show a velocity that is flat with v constant beyond the core of the galaxy, see Fig. 1.1. For example in our galaxy, $v \approx 220km/s$ at the Sun's location and does not vary much out to the largest observable radius.

In a galaxy one can relate the rotational velocity to the mass, M,

$$v(r) \propto \sqrt{\frac{G_N M(r)}{r}} \tag{1.5}$$

where G_N is the gravitational constant, $M(r) = 4\pi \int \rho(r) r^2 dr$ and $\rho(r)$ is the mass density profile. It should be $\propto 1\sqrt{r}$ beyond the optical disk. If the bulk of the mass was from luminous matter, M should be constant outside the luminous region and we should have $v^2 \propto 1/r$. The flat rotation curve indicates the presence of a dark

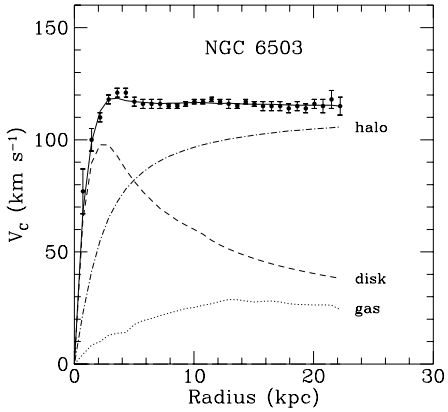

FIG. 1.1 – Rotation curve of NGC 6503. The dotted, dashed and dash-dotted lines are the contributions of the gas, disk and dark matter respectively. From Ref. [**?**].

halo, with mass density $\rho(r) = 1/r^2$ (so that $M \propto r$). Note that at some point ρ will have to fall off faster with r since the total mass of the galaxy has to be finite. The lower bound on the DM mass density from rotation curve is $\Omega_{DM} > 0.1$.

Observations of rotation curves also give information about the shape of dark matter halos. This can be done using Low Surface Brightness (LSB) galaxies which are believed to be everywhere dark matter dominated as the observed stellar population only make a small contribution to the rotation curves, A compilation of data **??** from 13 LSB galaxies suggest a shallow or even flat core. In fact rotation cuves of low and high surface luminosity galaxies suggest a universal density profile with an exponential thin stellar disk and a spherical dark matter halo with a flat core r_0 and density $\rho_0 = 4.5 \times 10^{-2}(r_0/kpc)^{-2/3} M_\odot$. On the other hand numerical N-body simulations find much steeper profiles that the ones inferred from observations. This remains a puzzle although claims have been made for reconciling observations with numerical simulations results.

1.1.2 Galaxy clusters

The first observations indicating that there was non-luminous matter were made in 1933 by a Swiss astronomer working at Caltech, Fritz Zwicky that measured mass-to-light ratios in galaxy clusters and from that inferred that most of the matter in the cluster was dark. For this he used the virial theorem which relates the average kinetic energy and average gravitational potential energy of bodies in a gravitationally

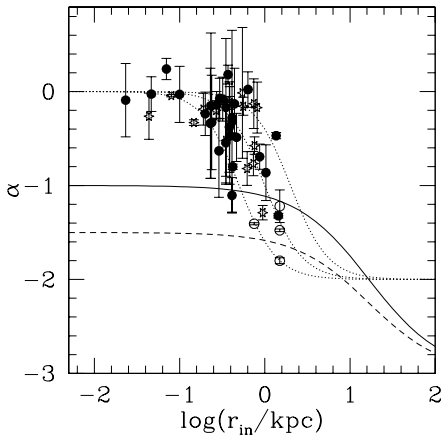

FIG. 1.2 – The value of α as a function of the radius of the innermost point. From Ref. [1].

bound system,

$$E_{K\,avg} = P_{avg} \tag{1.6}$$

To estimate the kinetic energy, one needs to measure the motions of bodies in the system. Using Doppler shift, the motion in the radial direction can be determined easily.

1.1.3 Gravitational lensing

Einstein's theory of relativity predicts that strong gravitational fields will bend the path of nearby light rays. This means that a very large mass can bend light rays and therefore becomes a lens (the lens is the gravitational field) hence it is called a gravitational lens.

A gravitational lens requires a very large mass, for example the mass of a galaxy, as well as a very distant light source behind it. Quasars are very distant objects in the Universe, furthermore they are very common. So it happens that a distant quasar is perfectly aligned with a galaxy, the galaxy acts as a gravitational lens and alter the image of the quasar. Numerous gravitational lens images of quasars have been observed.

Clusters of galaxies can also act as gravitational lenses. For example images of some clusters of galaxies show many blue arcs which are gravitational lens images of more distant background galaxies. Detailed study of these arcs allow astronomers

to measure the total mass of the cluster of galaxies. Observations show that only 10% of the total mass of the clusters are in the form of individual galaxies, the rest is dark matter.

1.1.4 Cosmology

The standard big-bang model of cosmology began in the 1940's with Gamow. With his collaborators Gamow proposed that the Universe was once very hot and dense and has expanded and cooled to its present state. Alpher and Herman predicted in 1948, as a direct consequence of this model, the existence of a relic background radiation with a temperature of a few K. This radiation, was discovered by chance by Penzias and Wilson in 1964. It is generally assumed that the Universe is homogeneous and isotropic. Observations of the Cosmic Microwave Background (CMB) have tested the isotropy hypothesis . Subsequent work on Big-Bang nucleosynthesis further confirmed the Big-Bang model. This model which relies on general relativity however faces problems with initial conditions, the best solution to this problem is inflationary cosmology.

The first ingredient of a cosmological model is the metric which describe the symmetry of the problem. Since the Universe is homogeneous and isotropic, the overall geometry can be described by two parameters taking into account the spatial curvature and the overall expansion of the Universe.

$$ds^2 = dt^2 - R^2(t)\left[\frac{dr^2}{1-kr^2} + r^2(d\theta^2 + \sin^2\theta d\phi^2)\right] \tag{1.7}$$

R is the cosmological scale factor, k is the three-space curvature constant ($k = 0, 1, -1$) for a flat, closed or open Universe.

The cosmological redshift, z, is a consequence of the Hubble expansion described by $R(t)$. A local observer detecting light from a distant emitter sees a redshift in frequency $z = \nu_1 - \nu_2/\nu_2$ where ν_1 is the frequency of the emitted light and ν_2 is the observed frequency. The redshift is simply related to the scale factor $1 + z = R_2/R_1$.

The cosmological equations of motions are derived from Einstein's equations that relate the geometry of the Universe to its matter and energy content,

$$\mathcal{R}_{\mu\nu} - \frac{1}{2}g_{\mu\nu}\mathcal{R} = 8\pi G_N T_{\mu\nu} + \Lambda g_{\mu\nu} \tag{1.8}$$

Assuming that the matter content of the Universe is a perfect fluid,

$$T_{\mu\nu} = -pg_{\mu\nu} + (p+\rho)u_\mu u_\nu \tag{1.9}$$

where p is the isotropic presseure, ρ is the energy density and $u = (1, 0, 0, 0)$ is the velocity vector for the isotropic fluid in co-moving coordinates. with a perfect fluid source, the Einstein equations lead to the FRW equation

$$H^2 = \left(\frac{\dot{R}}{R}\right)^2 = \frac{8\pi G_N \rho}{3} - \frac{k}{R^2} + \frac{\Lambda}{3} \tag{1.10}$$

where $H(t)$ is the Hubble parameter and Λ is the cosmological constant. Ignoring the cosmological constant, the Universe will recollapse in a finite time if $k = 1$ or will expand indefinitely for $k = 0, -1$. these can be modified when $\Lambda \neq 0$ or with some component with $\rho + 3p < 0$.

The Hubble parameter gives the slope of the relation between distance and recession velocity, it has been best measured by the Hubble Space Telescope and at present its value is $H(0) = H_0 = 73 \pm 3 \text{kms}^{-1}\text{Mpc}^{-1}$. The universe is flat in the absence of a cosmological constant and when the energy density equals the critical density, Eq. **??**. Defining the quantity $\Omega_i = \rho_i/\rho_c$ of a specie i with density ρ_i, we can write the Friedman nequation

$$(\Omega - 1)H^2 = \frac{k}{R^2} \tag{1.11}$$

so that $k = 0, 1, -1$ correspond to $\Omega = 1, \Omega > 1, \Omega < 1$. Note that Ω represents the sum of the matter density and the cosmological constant $\Omega = \Omega_m + \Omega_\Lambda$. Note that the various Ω_i evolve differently with time depending on the equation of state of the component.

In the last several years there has been huge progress in the determination of the cosmological parametesr. in particular through the analysis of the CMB. The CMB is known to be isotropic to the 10^{-5} level and to follow with very good precision the spectrum of a black body with a temperature of $T = 2.726\text{K}$. Information of the cosmological parameters are extracted from precise measurements of the CMB anisotropies.

The observed temperature anisotropies in the sky are expanded as

$$\frac{\delta T}{T}(\theta, \phi) = \sum_{l=2}^{\infty} \sum_{m=-l}^{l} a_{lm} Y_{lm}(\theta, \phi) \tag{1.12}$$

where $Y(l, m)(\theta, \phi)$ are spherical harmonics. The variance of a_{lm} is

$$C_l = \langle |a_{lm}|^2 \rangle = \frac{1}{2l+1} \sum_{m=-l}^{l} |a_{lm}|^2 \tag{1.13}$$

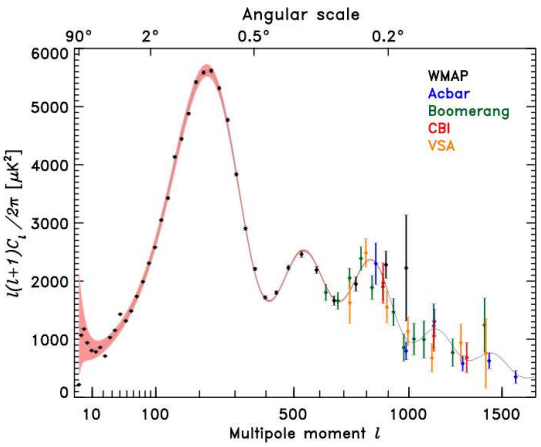

FIG. 1.3 – CMB measurement of the power spectrum.

If the temperature fluctuations are assumed to be Gaussian, all the information contained in CMB maps can be compressed into the power spectrum, this gives the behaviour of C_l as a function of l, see Fig. **??**. To extract information from the CMB maps one starts with a cosmological model with a fixed number of parameters and then fits the parameters from the peak in the N-dimensional likelihood surface. Cosmological paramters include h, the Hubble parameter, the different component of the density, $\Omega_m, \Omega_b, \Omega_\Lambda, \Omega_r, \Omega_\nu$, Δ^2_R, n that characterize density perturbations or how the Universe deviates from homogeneity, r the tensor to scalar ratio and τ the ionization optical depth that is related to the probability that a given photon scatters once.

The number of free parameters can be reduced by making a few simple assumptions. for example in inflation models one density parameter can be removed. Furthermore Ω_r can be fixed to the value measured directly by the COBE satellite. Finally CMB experiments are not very sensitive to r so this parameter can be ignored. The results of a fit to different cosmological parameters based on the CMB measurements by WMAP5 are listed in Table **??**, In particular this shows that there is a large dark energy (or cosmological constant) component. Furthermore the difference between the total matter content and the baryonic matter content indicates a strong dark matter component. Note that the baryonic component is consistent with the value extracted from BBN.

These can be combined with information from smaller scales, measurements on large scale structure and results from the Sloan Digital Sky Survey (SDSS) which measured the three-dimensional power spectrum of more than 200,000 galaxies. This gives in particular a determination of the matter density. In Supernovae there exist

TAB. 1.1 – Cosmological parameters extracted from WMAP and WMAP combined with SDSS and SNe. The ΛCDM model with a power-law initial spectrum, no tensors, spatial flatness and a cosmological constant as dark energy is assumed.

	WMAP5	WMAP5+SDSS+SNe
$\Omega_b h^2$	0.0227 ± 0.0006	0.0227 ± 0.0006
$\Omega_{cdm} h^2$	0.110 ± 0.006	0.113 ± 0.003
$\Omega_\Lambda h^2$	0.74 ± 0.03	0.726 ± 0.015
n	$0.963^{+0.014}_{-0.015}$	0.960 ± 0.013
τ	0.087 ± 0.017	0.084 ± 0.016
$\Delta^2_R \times 10^9$	2.41 ± 0.11	2.44 ± 0.10

a relation between the observed flux and intrinsic luminosity of an object this depends on the luminosity distance $D_L = (1+z)r_e(z)$ and in turn $r_e(z)$ depends on the cosmological paramters, in particular Ω_m and Ω_Λ. Observations of type 1a supernovae at high redshift thus allow to constrain a combination of Ω_m and Ω_{de} almost orthogonal to the one determined by WMAP. Combining these different results allows to refine the predictions for a few cosmological parameters including the cold dark matter density. The cosmological parameters will be further constrained by PLANCK which was launched in 2010.

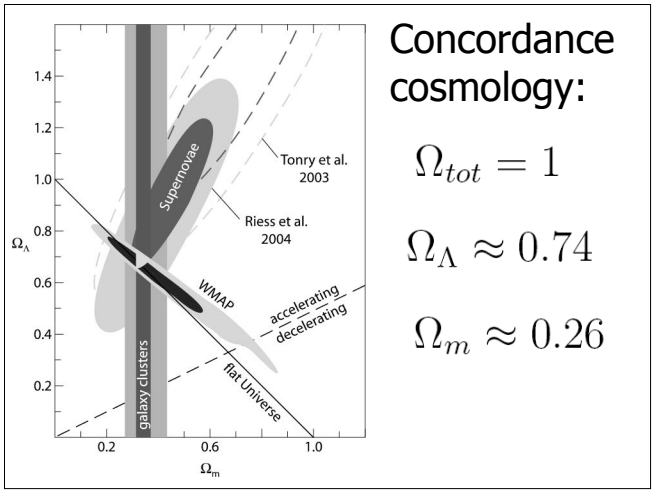

FIG. 1.4 – Measurements from CMB, large scale structure and supernovae in the Ω_Λ vs Ω_m plane [2]

1.1.5 Big-Bang Nucleosynthesis

Big-bang nucleosynthesis allows ro make predictions on the abundances of light elements $D, He^3, He^4,^7 Li$. It depends basically on only one parameter, η the baryon to photon ratio.

In the early Universe, energy density was dominated by radiation (from photons, electron/positrons and neutrinos) and conditions for synthesis of light elements were attained at $T \geq 1\text{MeV}/$ At these temperatures weak inteaction rates were in thermal equilibrium

$$\begin{aligned} n + e^+ &\rightarrow p + \nu \\ n + \nu &\rightarrow p + e^- \\ n &\rightarrow p + e^- + \nu_e \end{aligned} \tag{1.14}$$

the reverse process proceed at the same rate and the neutrion to proton ratio, $n/p \approx 1$. At lower temperatures weak interactions fall out of equilibrium and freeze out occurs when the interaction rate drops below the expansion rate, $\Gamma_{weak} < H$. The different species then decouple. When T approaches the point where weak interaction rates cannot maintain equilibrium $n/p \approx exp^{-\Delta m/T} \approx 1/6$. This orccurs around $T = 0.8\text{MeV}$. Note that neutron continue to decay so that $n/p \approx 1/7$.

Nucleosynthesis begins with formation of Deuterium $p + n \rightarrow D + \gamma$. Since the number of photons is much larger than the number of nucleons, $n_\gamma/n_B \approx 10^{-10}$, the reverse process occurs much faster, deuterium production is therefore delayed and starts only at $T \approx 0.1\text{MeV}$. The chain continues with production of heavier eleements. The main product of BBN is ^4He and its abundance depends sensitively on the neutron to proton ratio.

$$Y \approx \frac{2n/p}{1 + n/p} \approx 0.25 \tag{1.15}$$

Other elements are produced in lesser amounts with the abundance by number of $D,^3 He \approx 10^{-5}$ and $^7Li \approx 10^{-10}$ Combining predictions of BBN calculations with measurements of the abundances of $D,^4 He^7 Li$ one gets a conservative range of

$$5.1 \times 10^{-10} < \eta < 6.5 \times 10^{-10} \tag{1.16}$$

The baryon to photon ratio is related to $\Omega_b h^2$ [3]

$$\eta = 2.68 \times 10^{-8} \Omega_b h^2 \tag{1.17}$$

which leads to

$$0.019 < \Omega_b h^2 < 0.024 \tag{1.18}$$

This number is consistent with the value extracted from the CMB, $\Omega_b h^2 = 0.0227 \pm 0,0006$. This value is much below $\Omega_m h^2$ indicating that most of the matter must be non-baryonic. Note that the high precision of the value extracted from CMB means that this result can be used to 'predict' the light element abundances. The resulting D/H abundance and He abundances are in good agreement with observations while the Li abundance is in much poorer agreement with the one observed in the atmospheres of halo dwarf stars.

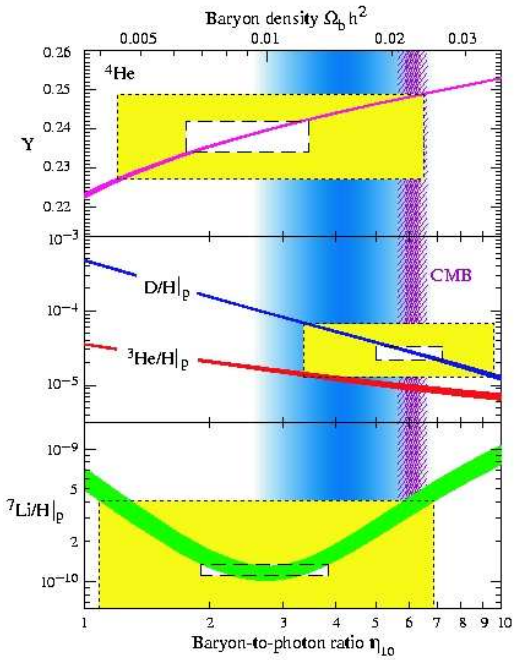

FIG. 1.5 – BBN predictions for the abundance of light elements as a function of the baryon to photon ratio η or $\Omega_b h^2$

1.1.6 Local dark matter density

The dark matter density in the neighbourhood of the Sun was first estimated by J.H. Jeans by analysing the motion of nearby stars transverse to the galactic plane. From that he concluded that in the solar neighbourhood the average density of DM must me roughly the same as that of luminous matter. Recent estimates based on detailed model of our galaxy find similar values $\rho_{DM} = 0.3 \frac{\text{GeV}}{\text{cm}^3}$

with roughly a factor of 2 uncertainty.

Chapitre 2

Relic density of dark matter

Suppose there exists a new stable (or very lond-lived) weakly-interacting massive particle (WIMP),χ, in addition to standard model particles. Such a particle is in thermal equilibrium in the early Universe when the temperature of the Universe is larger than the mass of the particle, m_χ. The equilibrium abundance is maintained by processes involving pair annihilation of the particle (and its antiparticle) into lighter standard model particles, for example

$$\chi\bar{\chi} \rightarrow e^+e^-, \mu^+\mu^-, \tau^+\tau^-, q\bar{q}, W^+W^-, ZZ \tag{2.1}$$

as well as the reverse processes. The WIMPs have enough energy to create pairs of SM particles and the inverse reaction proceeds with equal rate, $\Gamma_{ann} = \langle\sigma v\rangle n_{eq}$, where σv is the thermally averge cross section for annihilation of $\chi\bar{\chi}$ into lighter particles, v is the relative velocity of annihilating WIMPs, and n_{eq} is the the number density of the χ particles in thermal equilibrium.

The number density of a dilute weakly interacting particle is given by

$$n_\chi = \frac{g}{(2\pi)^3}\int f(\mathbf{p})d^3\mathbf{p} \tag{2.2}$$

Here g is the number of internal degrees of freedom of the particle and $f(\mathbf{p})$ is given by Fermi-Dirac or Bose-Einstein statistics

$$f(\mathbf{p}) = exp\left(\frac{E-\mu}{T} \pm 1\right)^{-1} \tag{2.3}$$

where μ is the chemical potential. With $E^2 = \mathbf{p}^2 + m^2$, the number density can be written as

$$n_\chi = \frac{g}{2\pi^2}\int_m^\infty \frac{(E^2-m^2)^{1/2}}{exp\left((E-\mu)/T\right) \pm 1} EdE \tag{2.4}$$

In the relativistic limit ($T \gg m_\chi$) and for $T \gg \mu$

$$\begin{aligned} n_\chi &= \frac{\zeta(3)}{\pi^2} g T^3 \quad \text{Bose} \\ n_\chi &= \frac{3}{4}\frac{\zeta(3)}{\pi^2} g T^3 \quad \text{Fermi} \end{aligned} \tag{2.5}$$

This means that $n_\chi^{eq} \propto T^3$ and there are about as many χ particles than photons. On the other hand at low temperatures, in the non relativistic limit $m \gg T$ and for $T \gg \mu$

$$n_\chi^{eq} \approx g(m_\chi T/2\pi)^{\frac{3}{2}} exp(-m_\chi/T). \tag{2.6}$$

The number density is Boltzmann suppressed. this means that if the expansion of the Universe was so slow that thermal equilibrium was always maintained then the number of WIMPs today would be exponentially suppressed (basically there would be no WIMPs). However equilibrium thermodynamics does not explain everything.

At $T \gg m_\chi$, the particle χ are abundant and rapidly annihilating to lighter particles and vice-versa. As the universe expands and T drops below m_χ the number density of χ drops exponentially, Eq. 2.6, and the rate of annihilation of χ, $\Gamma = \langle \sigma v \rangle$ drops below the expansion rate $\Gamma < H$. When there is not enough χ for annihilation, they fall out of equilibrium and they freeze-out (the production of WIMPs ceases). The number of WIMPs in a comoving volume remains constant. Typically the freeze-out of WIMPs occurs when $T \approx m_\chi/20$.

The Boltzmann equation describes the time evolution of the number density of WIMPs

$$\frac{dn_\chi}{dt} + 3Hn_\chi = -\langle \sigma v \rangle \left((n_\chi)^2 - (n_\chi^{eq})^2 \right) \tag{2.7}$$

The first term on the RHS describes the depletion of χ due to annihilation the second term the creation of χ from the inverse process. Note that at equilibrium the two rates are equal. $H = \dot{R}/R$ is the Hubble epansion rate, Eq. **??** with R the scale factor of the Universe.

2.1 The Boltzmann equation

The Boltzmann equation for the evolution of the phase space density, $f(E,t)$ of a particle specie can be derived starting from

$$L[f] = C[f] \tag{2.8}$$

where L is a Liouville operator that gives the rate of change in time of particle phase-space density and C is the collision operator, it represents the number of particles per phase space volume lost or gained after collision with other particles

$$L[f] = \frac{\partial f}{\partial t} - H\frac{|p|^2}{E}\frac{\partial f}{\partial E} \tag{2.9}$$

The number density is given in Eq. 2.6. To get the evolution equation for n, the Boltzmann equation is integrated over the particle momenta and summed over the spin degrees of freedom. Integrating by parts and using the fact that $E^2 = p^2 + m^2$, $EdE = pdp$, the left-hand side leads to

$$g_1 \int L[f_1]\frac{d^3p_1}{(2\pi)^3} = \frac{1}{R^3}\frac{d}{dt}(R^3 n_1) = \dot{n}_1 + 3Hn_1 \tag{2.10}$$

while the collision term in the simpler case of annihilation of 2 particles into 2 final states, $1 + 2 \to 3 + 4$, reads

$$\begin{aligned} g_1 \int C[f_1]\frac{d^3p_1}{(2\pi)^3} &= -\sum_{spins}\int \big(f_1 f_2(1 \pm f_3)(1 \pm f_4)|\mathcal{M}_{12\to 34}|^2 \\ &\quad - f_3 f_4(1 \pm f_1)(1 \pm f_2)|\mathcal{M}_{34\to 12}|^2\big) \\ &\quad (2\pi)^4\delta^4(p_1 + p_2 - p_3 - p_4)\Pi_1\Pi_2\Pi_3\Pi_4 \end{aligned} \tag{2.11}$$

where $\Pi_i = d^3p_i/((2\pi)^3 2E_i)$. The +(-) signs in $(1 \pm f_i)$ apply to bosons (fermions). Assuming that the annihilation products go quickly into equilibrium with the thermal background (this is a reasonable assumption since typically these particles have electromagnetic interactions with the thermal photons), we can replace f_3, f_4 by f_3^{eq}, f_4^{eq} and $1 \pm f_i \approx 1$. Furthermore because of the δ function in the integral, $f_3^{eq} f_4^{eq} = exp(-(E_3 + E_4)/T)$ can be replaced by $f_1^{eq} f_2^{eq} = exp(-(E_1 + E_2)/T)$. The unpolarized cross section for the scattering process $1 + 2 \to 3 + 4$ is defined as

$$\sigma_{12;34} = \frac{1}{4Fg_1g_2}\sum_{spins}\int |\mathcal{M}_{12\to 34}|^2(2\pi)^4\delta^4(p_1+p_2-p_3-p_4)\frac{d^3p_3}{(2\pi)^3 2E_3}\frac{d^3p_4}{(2\pi)^3 2E_4} \tag{2.12}$$

where $F = [(p_1 \cdot p_2)^2 - m_1^2 m_2^2]^{1/2}$. To include all processes one only needs to sum over all final states $\sigma = \sum_{XY}\sigma_{12\to XY}$ Furthermore T invariance implies that the integral over $|\mathcal{M}_{12\to 34}|^2$ equals $|\mathcal{M}_{34\to 12}|^2$ So that

$$g_1 \int C[f_1]\frac{d^3p_1}{(2\pi)^3} = -\int \sigma v g_1 g_2 \frac{d^3p_1}{(2\pi)^3}\frac{d^3p_2}{(2\pi)^3}(f_1 f_2 - f_1^{eq} f_2^{eq}) \tag{2.13}$$

Here $v = F/E_1E_2$ and is defined in such a way that vn_1n_2 is invariant under Lorentz transformations and is equal to the product of the relative velocity v_{lab} and the

particle densities in the rest frame of the one of the incoming particles. In terms of the particle velocities $v_1 = p_1/E_1$

$$v = \left[|v_1 - v_2|^2 - |v_1 \times v_2|^2\right]^{1/2} \tag{2.14}$$

Defining the thermally averaged total annihilation cross section

$$\langle \sigma v \rangle = \frac{\int d^3p_1 d^3p_2 f(E_1) f(E_2) \sigma v}{\int d^3p_1 d^3p_2 f(E_1) f(E_2)} \tag{2.15}$$

The collision term reads

$$g_1 \int C[f_1] \frac{d^3p_1}{(2\pi)^3} = -\langle \sigma v \rangle \left(n_1 n_2 - n_1^{eq} n_2^{eq}\right) \tag{2.16}$$

and we obtain

$$\dot{n}_1 + 3Hn_1 = -\langle \sigma v \rangle (n_1 n_2 - n_1^{eq} n_2^{eq}) \tag{2.17}$$

with the same expression for n_2. If the two particles are identical $n = n_1 = n_2$, and we obtain the Boltzmann equation, Eq. 2.7.

2.2 Thermally averaged cross section

When the initial particle have an energy distribution $f(E)$ the thermally averaged cross section for annihilation of two particles into i final states is defined in Eq. 2.15. Since we know that the particle density of χ particles will depart from equilibrium only after T falls below $M/20$, at these temperature it is a good approximation to take $f(E) \propto exp^{-E/T}$, the Maxwell-Boltzmann distribution, A few manipulations allow to rewrite the thermally averaged cross section, Eq. 2.15. First write integration variables

$$d^3p_1 d^3p_2 = 4\pi p_1 dE_1 4\pi p_2 dE_2 \frac{1}{2} d\cos\theta \tag{2.18}$$

where θ is the angle between p_1 and p_2. After a change of variable

$$E_+ = E_1 + E_2 \quad E_- = E_1 - E_2 \tag{2.19}$$

and

$$s = 2m^2 + 2E_1E_2 - 2p_1p_2\cos\theta \tag{2.20}$$

$$d^3p_1 d^3p_2 = 2\pi^3 E_1 E_2 dE_+ dE_- ds \tag{2.21}$$

The integration regions ($E_1 > m, E_2 > m; |\cos\theta| < 1$) transforms to

$$|E_1| \leq \sqrt{1 - \frac{4m^2}{s}} \sqrt{E_+^2 - s} \quad E_+ \geq \sqrt{s} \quad s \geq 4m^2 \tag{2.22}$$

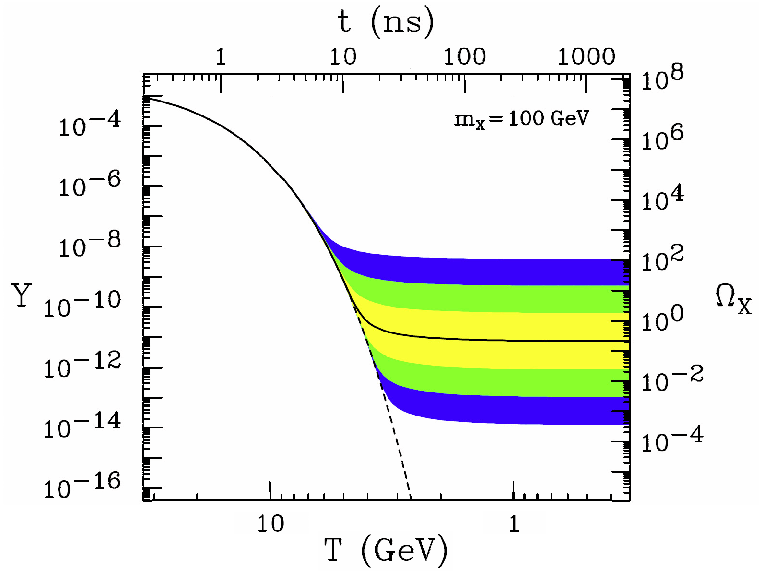

FIG. 2.1 – Evolution of the WIMP number density in the early Universe from Ref. [4]. the contours correspond to cross sections enhanced by a factor 10,100 and 1000.

The numerator in Eq. 2.15 becomes

$$\begin{aligned} Num &= 2\pi^2 \int dE_+ \int dE_- \int ds \sigma v E_1 E_2 exp^{-E_+/T} \\ &= 4\pi^2 \int ds \sigma F \sqrt{1 - \frac{4m^2}{s}} \int dE_+ exp^{-E_+/T} \sqrt{E_+^2 - s} \\ &= 2\pi^2 T \int ds \sigma (s - 4m^2) \sqrt{s} K_1 \left(\sqrt{s}/T\right) \end{aligned} \tag{2.23}$$

where K_n is the modified Bessel function os the second kind of order n. Note that the integration on E_+ could be performed because $\sigma F = \sigma v E_1 E_2$ is a function of s only. We have used $F = 1/2\sqrt{s(s-4m^2)}$. For the denominator of Eq. 2.15 we get

$$\int d^3p_1 d^3p_2 f(E_1) f(E_2) = \left[4\pi m^2 T K_2(m/T)\right]^2 \tag{2.24}$$

Thus

$$\langle \sigma v \rangle = \frac{1}{8m^4 T K_2^2(m/T)} \int_{4m^2}^{\infty} \sigma (s - 4m^2) \sqrt{s} K_1(\sqrt{s}/T) ds \tag{2.25}$$

This result is general and works even near threshold and resonances when the frequently used simplified equation where σv is expanded in powers of v fails.

2.3 Solving the Boltzmann equation

To put the equation 2.7 in a more convenient form we consider Y the ratio of the number density to the entropy density s.

$$\frac{dY}{dt} = \frac{d}{dt}\left(\frac{n}{s}\right) = \frac{dn}{dt}\frac{1}{s} - \frac{n}{s^2}\frac{ds}{dt} \tag{2.26}$$

In the absence of entropy production $R^3 s$ is a constant so that

$$\frac{ds}{dt} = -3Hs \tag{2.27}$$

and

$$\frac{dY}{dt} = \frac{dn}{dt}\frac{1}{s} + 3H\frac{n}{s} \tag{2.28}$$

so the evolution equation can be rewritten as

$$\frac{dY}{dt} = -s\langle\sigma v\rangle\left(Y^2 - Y_{eq}^2\right) \tag{2.29}$$

The right hand side depends only on temperature so it is more convenient to use temperature instead of time. Using

$$\frac{ds}{dT}\frac{dT}{dt} = -3Hs \tag{2.30}$$

$$\frac{dY}{dT} = \frac{1}{3H}\frac{ds}{dT}\langle\sigma v\rangle\left(Y^2 - Y_{eq}^2\right) \tag{2.31}$$

Defining a new variable $x = m/T$,

$$\frac{dY}{dx} = -\frac{m}{x^2}\frac{1}{3H}\frac{ds}{dT}\langle\sigma v\rangle\left(Y^2 - Y_{eq}^2\right) \tag{2.32}$$

In a radiation dominated universe with the Friedmann-Robertson-Walker cosmology, the Hubble parameter is

$$H^2 = \frac{8\pi G\rho}{3} \tag{2.33}$$

where ρ is the total energy density of the Universe. The energy and entropy density can be parameterized in terms of the effective degrees of freedom g_{eff} and h_{eff}

$$\rho = g_{eff}(T)\frac{\pi^2}{30}T^4 \quad s = h_{eff}(T)\frac{2\pi^2}{45}T^3 \tag{2.34}$$

where $g_{\rm eff}(T) = h_{\rm eff} = 1$ for a relativistic specie with one degree of freedom. $h_{\rm eff}$ is a function that depends slowly on the temperature T [5]. Replacing Eq. 2.34 and 2.33 in Eq. 2.32, the evolution equation of Y becomes

$$\frac{dY}{dx} = -\sqrt{\frac{\pi g_*(T)}{45G}}\frac{m}{x^2} < \sigma v > (Y^2 - Y_{eq}^2) \tag{2.35}$$

$g_*(T)$ is a degree of freedom parameter derived from the thermodynamics describing the state of the universe [5, 6]

$$g_*^{1/2} = \frac{h_{\rm eff}}{g_{\rm eff}^{1/2}}\left(1 + \frac{1}{3}\frac{T}{h_{\rm eff}}\frac{dh_{\rm eff}}{dT}\right) \tag{2.36}$$

and $Y_{eq} = Y_{eq}(T)$ represents the thermal equilibrium abundance

$$Y_{eq}(T) = \frac{n_{eq}}{s} = \frac{45}{4\pi^4 h_{eff}(T)}\, g\frac{m^2}{T^2}K_2\left(\frac{m}{T}\right) \tag{2.37}$$

that can be directly obtained from Eq. **??**. Note that Y_{eq} falls rather rapidly as the temperature decreases. This equation is valid under the conditions that annihilation processes are in thermal equilibrium, the chemical potential is negligible. The temperature dependence of $g_*^{1/2}$ is shown in Fig. **??**, for a complete description on how to derive $g_*^{1/2}$ see [7] and references therein.

Integrating Eq. 2.35 from $T = \infty$ to $T = T_0$ where T_0 is the photon temperature of the Universe today, would lead Y_0, see description below. The relic density at present in units of the critical density can be expressed as

$$\Omega_\chi = \frac{m_\chi n_\chi}{\rho_{\rm crit}} = \frac{m_\chi s_0 Y_0}{\rho_{\rm crit}} \tag{2.38}$$

where $\rho_{\rm crit}$ is defined in Eq. **??** and $s_0 = s(T_0)$ defines today's entropy to be evaluated at $T_0 = 2.726K$, the temperature of the microwave background. Assuming that $h_{eff} = 3.91$ corresponding to photons and 3 Dirac neutrinos, then $s_0 = 2889.2{\rm cm}^{-3}$. $m_{\tilde{\chi}_1^0}$ is the mass of the WIMP, $H = 100h$ kms$^{-1}Mpc^{-1}$ is the Hubble constant and $G_N^{-1/2} = M_{Pl} = 1.22 \times 10^{19}$GeV the Newton constant. Substituting the numerical values, one obtains the relic density

$$\Omega_\chi h^2 = 2.755 \times 10^8 \frac{m_\chi}{GeV} Y_0 \tag{2.39}$$

Note that 1pc $= 3.08 \times 10^{16}$m and 1eV $= 1.782 \times 10^{-36}$kg.

2.3.1 The freeze-out approximation

One can solve for Y numerically or use the freeze-out approximation. At high T, the WIMP are very close to equilibrium and thus $Y \simeq Y_{eq}$. This will hold until freeze-out, where Y will be almost constant whereas Y_{eq} will decrease significantly. At high T, one can make the approximation that $d(Y - Y_{eq})/dT$ is negligible. The freeze-out temperature T_f can be defined from $Y_f = Y(T_f) = (1+\delta)Y_{eq}(T_f)$ with δ some (small) constant number, T_f can then be extracted by solving

$$\frac{dln(Y_{eq})}{dT} = \sqrt{\frac{\pi g_*(T)}{45G}} < \sigma v > Y_{eq}\delta(\delta+2) \tag{2.40}$$

Th equation is solved iteratively, a good starting point is $T_f = m/25$ and only a few iterations are necessary to find a solution with $\delta \approx 1.5$. In the second regime, where $Y \gg Y_{eq}$, one can neglect Y_{eq}^2 completely. One finds[7]

$$\frac{1}{Y(0)} = \frac{1}{Y_f} + \sqrt{\frac{\pi}{45G}} \int_{T_0}^{T_f} g_*^{1/2}(T) < \sigma v > dT \quad , \tag{2.41}$$

The two solutions are then matched at $T = T_f$.

2.3.2 An approximate solution

The χ particles freeze out at a temperature $T_f \approx m_\chi/20$ this means that the particles are non-relativistic ($v \ll 1$) when they freeze out. We can expand the annihilation cross section

$$\sigma v = a + bv^2 \tag{2.42}$$

where v is the relative velocity. The first term comes from s-wave ($L = 0$) annihilation while bv^2 comes from s- and p-wave annihilation ($L = 1$). If a were dominant σv would be energy independent, however in many cases, for example for Majorana particle, the s-wave annihilation into light fermions is helicity suppressed and bv^2 must be taken into account.

In most cases only the first two terms in the expansion are needed and the evolution equation is solved approximately. After thermal averaging

$$\langle \sigma v \rangle = a + 6bT/m \tag{2.43}$$

Neglecting $1/Y_f$ in Eq. 2.41 and assuming that g_* varies slowly with temperature we get

$$Y_0^{-1} = \sqrt{\frac{\pi}{45G_N}} \int g_*^{1/2} \langle \sigma v \rangle dT \tag{2.44}$$

the term in the integral is roughly $g_*^{1/2}(T_f)\langle\sigma v\rangle T_f$ (if σv is dominated by b term one gets an additional factor of 1/2). Replacing the numerical values in Eq. **??** we get an order of magnitude estimate

$$\begin{aligned}\Omega h^2 &= 2.755\times 10^8 GeV^{-1} x_F \sqrt{\frac{45}{\pi}} \frac{x_F}{M_{Pl} g_*^{1/2}\langle\sigma v\rangle} \\ &= \frac{2.755\times 10^8 GeV^{-1}}{1.2\times 10^19 GeV}\sqrt{\frac{45}{\pi}} 0.389 GeV^2 mb\times 10^{-27} cm^2/mbc \left(\frac{x_F}{g_*^{1/2}\langle\sigma v\rangle}\right) \\ &= 1.07\times 10^{-27}\left(\frac{x_F}{g_*^{1/2}\langle\sigma v\rangle}\right) \approx \frac{3\times 10^{-27}\mathrm{cm^3 s^{-1}}}{\langle\sigma v\rangle} \end{aligned} \tag{2.45}$$

The typical annihilation cross section at freeze-out to get the value of Ωh^2 extracted from WMAP measurements is therefore $\langle\sigma v\rangle = 3\times 10^{-26} cm^3/sec$. This is a "typical" cross section for weak interactions at a scale of 100GeV and has provided strong motivation for considering WIMPs as prime dark matter candidates.

Note that while allowing for a straigthforward solution to the evolution equation and the relic density, the expansion of the annihilation cross section in v is not always valid. In particular it fails when annihilation is dominated by a resonance or when it occurs near a threshold, for example near the threshold for W pair production. There are several public codes that provide complete and accurate numerical solutions to the Boltzmann equation in supersmmetric extensions of the standard model (DarkSUSY [8], IsaTools [9], superISOrelic [10]) or in generic extensions of the standard model (micrOMEGAs [11]).

2.4 Coannihilation

Take N non-standard particles with mass m_i and internal degrees of freedom g_i, the lightest of these particles is stable if protected by a symmetry, we call this particle LSP (Lightest Stable Particle), χ_1. The relic abundance of the lightest particle is determined not only by its annihilation cross section but also by the annihilation of the heavier particles. Since these heavier particles will later all decay into the lightest one. This is called coannihilation [12]. As we will see coannihilation is relevant only when the mass difference between χ_1 and χ_i is small.

Three types of reactions change the number densities of χ_i, $\chi_i\chi_j \to XY$, $\chi_i X \to \chi_j Y$ and $\chi_j \to \chi_i XY$ where X, Y stand for any SM particle. The abundances of χ_i are determined by a set of N Boltzmann equations

$$\begin{aligned}\frac{dn_i}{dt} &= -3Hn_i - \sum_{i,j=1}^{N} \langle \sigma_{ij} v_{ij} \rangle \left(n_i n_j - n_i^{eq} n_j^{eq} \right) \\ &\quad - \sum_{j \neq i} \langle \sigma'_{Xij} v_{ij} \rangle \left(n_i n_X - n_i^{eq} n_X^{eq} \right) - \sigma'_{Xji} v_{ij} \rangle \left(n_j n_X - n_j^{eq} n_X^{eq} \right) \\ &\quad - \sum_{j \neq i} \left(\Gamma_{ij} (n_i - n_i^{eq}) - \Gamma_{ji} (n_j - n_j^{eq} \right) \end{aligned} \tag{2.46}$$

where n_X are the number densities of the SM particles involved in the reactions. These particles are assumed to be light and thus relativistic at freeze-out.

The second term on the RHS describes $\chi_i \chi_j$ annihilations,

$$\sigma_{ij} = \sum_{SM} \sigma(\chi_i \chi_j \to X_{SM} X_{SM}) \tag{2.47}$$

σ_{ij} is the total cross section for $\chi_i \chi_j$ annihilation into all possible SM final state. The relative velocity is

$$v_{ij} = \frac{\left((p_i \cdot p_j)^2 - m_i^2 m_j^2 \right)^{1/2}}{E_i E_j} \tag{2.48}$$

The third term in Eq. 2.46 corresponds to scattering off the cosmic thermal background $\chi_i X \to \chi_j Y$ and

$$\sigma'_{Xij} = \sum_{X,Y} \sigma(\chi_i X_{SM} \to \chi_j Y_{SM}), \tag{2.49}$$

The last term describes χ_i decays with $\Gamma_{ij} = \sum_X \Gamma(\chi_i \to \chi_j X_{SM})$. The equilibrium number density is defined as before, Eq. 2.6 and so is the thermal average

$$\langle \sigma_{ij} v_{ij} \rangle = \frac{\int d^3 p_i d^3 p_j f(E_i) f(E_j) \sigma_{ij} v_{ij}}{\int d^3 p_i d^3 p_j f(E_i) f(E_j)} \tag{2.50}$$

Normally the decay rate of the new particles χ_i other than the LSP is much faster than the decay rate of the Universe, so all these particles will decay into the lightest one. The abundance of the LSP is thus given by the sum of the density of the N new particles.

$$n = \sum_{i=1}^{N} n_i \tag{2.51}$$

The equation for the number density, Eq. 2.6 becomes

$$\frac{dn}{dt} = -3Hn - \sum_{i,j=1}^{N} \langle \sigma_{ij} v_{ij} \rangle \left(n_i n_j - n_i^{eq} n_j^{eq} \right) \tag{2.52}$$

since the last terms in Eq. 2.46 cancel in the sum. The scattering rate for new particles on SM particles in the thermal background is much faster than their annihilation rate. Indeed the cross sections σ'_{Xij} are of the same order as σ_{ij} but the density n_X of relativistic particles is much larger than the density n_i of non-relativistic particles which are Boltzmann suppressed.

$$n_i n_j \sigma_{ij} \propto T^3 m_i^{3/2} m_j^{3/2} \sigma_{ij} exp^{-(m_i+m_j)/T} \tag{2.53}$$

while

$$n_i n_X \sigma'_{Xij} \propto T^{9/2} m_i^{3/2} \sigma'_{ij} exp^{-m_i/T} \tag{2.54}$$

Assuming similar cross sections it means that the latter are larger by a factor

$$n_X / n_j \propto (T/m_j)^{3/2} exp^{m_j/T} \approx 10^9 \tag{2.55}$$

for a freeze-out temperature $T_f \approx m_\chi/20$. The χ_i particles thus remain in thermal equilibrium, in particular the ratios of densities are equal to the equilibrium values before during and after freeze-out

$$\frac{n_i}{n} \approx \frac{n_i^{eq}}{n^{eq}} \tag{2.56}$$

For convenience we define

$$r_i = \frac{n_i^{eq}}{n^{eq}} = \frac{g_i (1+\Delta_i)^{3/2} exp(-x_i \Delta_i)}{g_{eff}} \tag{2.57}$$

where

$$\Delta_i = \frac{m_i - m_1}{m_1} \tag{2.58}$$

and

$$g_{eff} = \sum_{i=1}^{N} g_i (1+\Delta_i)^{3/2} exp(-x\Delta_i) \tag{2.59}$$

Then

$$\frac{dn}{dt} = -3Hn - \langle \sigma_{eff} v \rangle \left(n^2 - n_{eq}^2 \right) \tag{2.60}$$

where

$$\begin{aligned}\sigma_{eff} &= \sum_{ij}^{N} \sigma_{ij} r_i r_j \\ &= \sum_{ij}^{N} \sigma_{ij} \frac{g_i g_j}{g_{eff}^2} (1+\Delta_i)^{3/2} (1+\Delta_j)^{3/2} exp^{-x(\Delta_i+\Delta_j)} \end{aligned} \tag{2.61}$$

and

$$\langle \sigma_{eff} v \rangle = \sum_{ij} \langle \sigma_{ij} v_{ij} \rangle \frac{n_i^{eq}}{n^{eq}} \frac{n_j^{eq}}{n^{eq}} \tag{2.62}$$

Following the same steps as above for the thermal average, we find the complete expresssion

$$< \sigma_{eff} v >= \frac{\sum\limits_{i,j} g_i g_j \int\limits_{(m_i+m_j)^2} ds \sqrt{s} K_1(\sqrt{s}/T) p_{ij}^2 \sigma_{ij}(s)}{2T\big(\sum\limits_i g_i m_i^2 K_2(m_i/T)\big)^2} , \tag{2.63}$$

where σ_{ij} is the total cross section for annihilation of a pair of supersymmetric particles into some Standard Model particles, and p_{ij} is the momentum of the incoming particles in their center-of-mass frame.

$$p_{ij} = \frac{1}{2} \left[\frac{(s-(m_i+m_j)^2)(s-(m_i-m_j)^2)}{s} \right]^{\frac{1}{2}} \tag{2.64}$$

The summation is over all N particles. Starting from these equations one can then proceed as for the case of only one LSP to solve for the abundance and obtained the relic abundance.

The generalisation of Eq. 2.37

$$Y_{eq}(T) = \frac{n_{eq}}{s} = \frac{45}{4\pi^4 h_{eff}(T)} \sum_i g_i \frac{m_i^2}{T^2} K_2(\frac{m_i}{T}) \tag{2.65}$$

where we sum over all supersymmetric particles i with mass m_i and g_i degrees of freedom.

In later chapters when we discuss specific dark matter particles we will see several examples where coannihilation plays an important role. Coannihilation processes are strongly suppressed if there is a large mass difference with the LSP. For example

for processes $\chi_i\chi_1 \to XX$ the suppression factor is $exp(-20(m_j - m_1)/m_1) \approx 0.02$ for a 20% mass difference. Larger mass differences can be relevant if the typical cross section of the coannihilation process is much larger than the dominant process (this can be the case for example when coannihilation involve strongly interacting particles or when coannihilation process benefits from a resonance effect). Note that coannihilation includes not only process involving $\chi_1\chi_j$ but also $\chi_i\chi_j$. The latter have a further Boltzmann suppression factor but in many cases have much larger cross sections.

Chapitre 3

Dark matter searches

There are two types of particle astrophysics experiments that search for dark matter : direct and indirect searches. These experiments will be described in the second part of the course. Here we introduce some theoretical aspects of dark matter searches and summarise the status of dark matter searches as will be required for the following discussion when we examine dark matter candidates.

3.1 Indirect detection

Pairs of dark matter particles present in the galactic halo can annihilate into standard particles. These further decay and hadronise leading to stable particles such as γ e^+ $\bar{p}$ or neutrinos that can be searched for in cosmic rays. The rate for production of SM particles is

$$Q(x, E) = \frac{\langle \sigma v \rangle}{2} \left(\frac{\rho(x)}{m_\chi} \right)^2 \frac{dN}{dE} \tag{3.1}$$

where $\langle \sigma v \rangle$ is the cross section for annihilation of DM particles into SM particles and $v \approx 0.001c$ is the typical velocity of WIMPs, $\rho(x)$ is the DM spatial distribution, m_χ the mass of the DM and dN/dE is the energy spectrum of the particle produced. This energy spectrum is fully calculable and does depend on the specific annihilation channels involved. For example the positron spectrum originating from W's is harder than the one originating from b quarks. These spectra are computed and tabulated for different masses of DM particles and for each of the standard annihilation channels. σ is the same quantity that enters the computation of the

relic density, it depends on the details of the particle physics model. Note however that v is much smaller than the one entering the relic density computation so that channels that are dominated by b in $\sigma = a + bv^2$ will be strongly suppressed here.

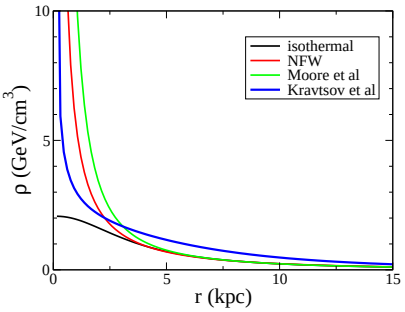

FIG. 3.1 – The halo profile as a function of r.

The photon flux is simply given by

$$\frac{d\phi_\gamma(E)}{dE} = \frac{1}{8\pi}\left(\frac{\langle\sigma v\rangle}{m_{\chi 0}}\right)^2 \sum_i BR_i \frac{dN_i}{dE} \int dl(\psi)\, \rho^2_{\chi_0}(l(\psi)) \tag{3.2}$$

where BR_i is the fraction into a given SM final state i, dN_i/dE is the number of photons produced after hadronization in terms of the energy E, $l(\psi)$ is the line of sight in the ψ direction. Since the dark matter spatial distribution is a quantity that has large uncertainties in the center of galaxies, see Fig. **??** it can introduce orders of magnitudes uncertainties in the prediction for the flux of photons from the center of the galaxy. On the other hand all halo model have similar predictions away from the center, in particular FermiLAT are imposing upper limits on σv from DM annihilation, the best limits are obtained for observations of dwarf galaxies and are slightly above the expectations of typical dark matter models that are consistent with WMAP, see Fig. where the predictions of the MSSM are also displayed.

The charged particles generated from DM annihilation propagate through the Galactic halo and their energy spectrum at the Earth differs from the one produced at the source. Charged particles are deflected by the irregularities of the galactic magnetic field. In the Milky Way which has strong magnetic turbulence Monte Carlo simulations indicate that this is described by space diffusion. Charged particles also suffer energy losses from synchroton radiation and inverse Compton scattering as well as diffusive reacceleration in the disk (which will be neglected below). Finally galactic convection wipes away charged particles from the disk. Solar modulation can also affect the low energy part of the spectrum. The equation that describes the evolution

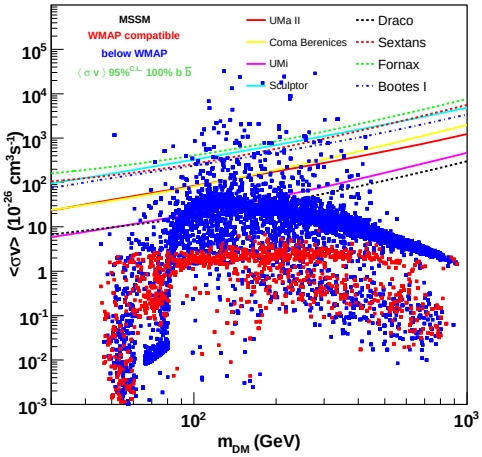

FIG. 3.2 – Limits on σv vs the DM mass from observations of dwarf galaxies by Fermi-LAT. The predictions of the MSSM are also displayed.

of the energy distribution for all particles (protons, anti-protons, positrons) reads

$$\frac{\partial}{\partial z}\left(V_C \psi_a\right) - \nabla \cdot \left(K(E) \nabla \psi_a\right) - \frac{\partial}{\partial E}\left(b(E) \psi_a\right) = Q_a(\mathbf{x}, E) \tag{3.3}$$

where $\psi_a = dn/dE$ is the number density of particles per unit volume and energy, a denotes the particle specie, V_C is the convective velocity and Q_a is the source term. The source term contains particles produced from dark matter annihilation as well as the background from conventionnal sources. K is the space diffusion coefficient, assumed homogeneous.

$$K(E) = K_0 \beta(E) \left(\mathcal{R}/1 \text{ GV}\right)^{\delta} \tag{3.4}$$

where β is the particle velocity and $\mathcal{R} = p/q$ its rigidity. $b(E)$ is the energy loss rate. The simple power law for $K(E)$ is inferred from magnetohydrodynamics considerations [**?**]. The parameters entering the propagation equation are set so that they reproduce the correct ratio for the abundance of B/C [13] as well as the observed spectra of antiparticles. This still leaves a large uncertainty in the computation of the background, see Fig. 3.3a.

Different experiments have been running and many results were presented recently, notably by PAMELA, Fermi-LAT and HESS. Furthermore AMS2 was launched in May 2011 and will also probe cosmic rays and dark matter. PAMELA, a satellite that detects positrons and antiprotons, has measured a rise in the positron fraction spectrum, while the antiproton spectrum fits very well the theoretical expectations from background only. The rise was recently confirmed by Fermi-LAT []. Interpreting this rise as a sign of DM raises some issues at many levels since the signal is not

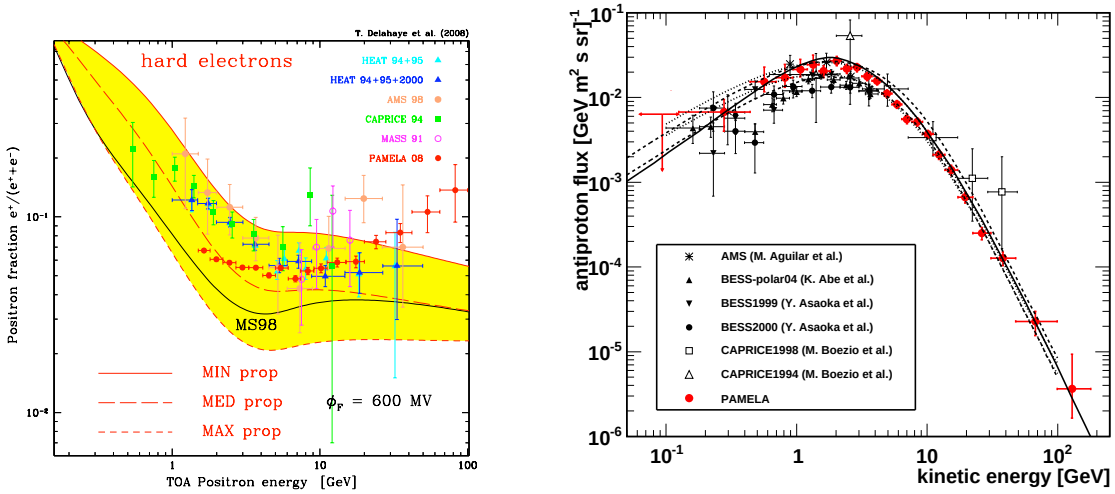

FIG. 3.3 – a) The theoretical prediction of the positron fraction as a function of energy for different propagation models, from [14] as compared to various measurements. b) The antiproton flux as a function of energy [15].

only very large (the typical cross section necessary to fit the data is many orders of magnitude above the typical $\sigma v = 3 \times 10^{-26} cm^3/s$) but occurs only for positrons. In most WIMP interpretations, one would expect an accompanying signal in antiprotons and photons . The measurements of the antiproton flux from PAMELA, see Fig. 3.3b, shows no excess over the expected background. A possible explanation could be that astrophysical sources such as pulsars rather than DM are responsible for these signals.

3.2 Direct detection

In direct detection, one measures the recoil energy deposited by the scattering of WIMPs with the nuclei in a large detector. A confirmed signal will thus offer strong evidence that WIMPs are indeed the DM. Generically WIMP-nuclei interactions can be split into spin independent (scalar) and spin dependent interations. The scalar interactions add coherently in the nucleus so heavy nuclei offer the best sensitivity. On the other hand, spin dependent interactions rely mainly on one unpaired nucleon and therefore dominate over scalar interactions only for light nuclei. In both cases, the cross-section for the WIMP nuclei interaction is typically low, so large detectors are required. Background rejection is clearly an important issue. Many experiments

involving a variety of nuclei have been set up or are being planned. Detectors made of heavy nuclei (for example Germanium or Xenon) currently in operation include Edelweiss [16], DAMA [17], CDMS [18], Xenon [19], CoGeNT []..... Upgrades and new detectors have been proposed as well. Detectors made of light nuclei which are sensitive mainly to the spin dependent interaction include Picasso [20], COUPP [] and KIMS [21] Signals have been reported in DAMA [22], CoGeNT and CDMS but remain to be confirmed while the best exclusion for spin-independent interactions are set by CDMS and Xenon [23].

Many ingredients enter the calculation of the direct detection rate and cover both astroparticle, particle and nuclear physics aspects. The detection rate depends of course on the WIMP nucleus cross section. These are obtained from the WIMP nucleon cross sections after folding in the nuclei form factors. The WIMP nucleon cross sections in turn is related at the more fundamental level to the WIMP quark interaction. At the particle physics level the process involves the scattering of dark matter particle on quarks and gluons that form the nucleons. Finally the rate will depend on the WIMP density near the Earth and on the velocity distributino in the galactic halo. We will describe in the following the different steps in the computation of the elastic scattering rate of WIMPs on nuclei.

In the non-relativistic limit, WIMP-nucleon elastic amplitudes can be divided into two classes, the scalar or spin independent interaction and the axial-vector or spin dependent interaction. We will start our presentation with the case of spin independent scattering of a Majorana WIMP before covering spin dependent interactions. In both cases the theoretical uncertainties involved will be discussed.

3.2.1 Spin independent interactions of Majorana fermions

To describe the interaction of WIMPs with nucleons we will use the language of effective Lagrangian, this approach is motivated by the fact that interactions can be computed in the limit of zero momentum transfer. Indeed the momentum transfer

$$\sqrt{-Q^2} = 2v\frac{m_{\tilde{\chi}}M_A}{m_{\tilde{\chi}} + M_A} \tag{3.5}$$

is much smaller than the masses of the WIMP or nuclei, since the velocity the velocity of dark matter particles near the Earth is of the order of the orbital velocity of the Sun $v \approx 0.001c$. Typically $Q^2 = 100\text{MeV}$ for $M_A \approx m_{\tilde{\chi}} \approx 100\text{GeV}$.

The most general effective Lagrangian for a Majorana fermion reads [24]

$$\begin{aligned}\mathcal{L}_F &= \lambda_N \overline{\psi}_\chi \psi_\chi \overline{\psi}_N \psi_N + i\kappa_1 \overline{\psi}_\chi \psi_\chi \overline{\psi}_N \gamma_5 \psi_N + i\kappa_2 \overline{\psi}_\chi \gamma_5 \psi_\chi \overline{\psi}_N \psi_N + \kappa_3 \overline{\psi}_\chi \gamma_5 \psi_\chi \overline{\psi}_N \gamma_5 \psi_N \\ &+ \kappa_4 \overline{\psi}_\chi \gamma_\mu \gamma_5 \psi_\chi \overline{\psi}_N \gamma^\mu \psi_N + \xi_N \overline{\psi}_\chi \gamma_\mu \gamma_5 \psi_\chi \overline{\psi}_N \gamma^\mu \gamma_5 \psi_N \end{aligned} \tag{3.6}$$

In the zero momentum transfer limit the operator $\overline{\psi}\gamma_5\psi$ vanishes while only the space component of $\overline{\psi}\gamma_5\gamma_\mu\psi$ and the time component of $\overline{\psi}\gamma_\mu\psi$ remain. Thus the operators κ_i are suppressed by factors of order q^2/m_N^2 and/or q^2/m_χ^2. Only one operator survives respectively for scalar (spin-independent) interactions, λ_N and for spin dependent interactions, ξ_N.

For spin-independent (SI) interactions with nucleons the effective Lagrangian thus simplifies to

$$\mathcal{L}^{SI} = \lambda_N \overline{\psi}_\chi \psi_\chi \overline{\psi}_N \psi_N \tag{3.7}$$

where $N = p, n$. The squared amplitude for a nucleon after averaging (summing) over the polarization of incoming (outgoing) particles is,

$$|A_N^{SI}|^2 = 64 \left(\lambda_N M_\chi M_N\right)^2 \tag{3.8}$$

where M_N is the nucleon mass. Summing on proton and neutron amplitudes gives for WIMP-nucleus interaction at rest,

$$|A_A^{SI}|^2 = 64 M_\chi^2 M_A^2 (\lambda_p Z + \lambda_n (A - Z))^2 \tag{3.9}$$

where Z is the nucleus charge and A the total number of nucleons. It leads to the cross section for a WIMP scattering at rest from a point-like nucleus

$$\sigma_0^{SI} = \frac{4\mu_\chi^2}{\pi} \left(\lambda_p Z + \lambda_n (A - Z)\right)^2 \tag{3.10}$$

where μ_χ is the WIMP-nucleus reduced mass, $\mu_\chi = m_{\tilde{\chi}} M_A/(m_{\tilde{\chi}} + M_A)$. Note that the nucleon cross-section add coherently so that for large nuclei there is an enhancement proportionnal to A^2 when $\lambda_p \approx \lambda_n$.

The matrix elements for WIMP nucleon interactions are related to the more fundamental matrix elements for WIMP quarks interactions. The effective operators for quarks are similar to the nucleon operators, Eq. 3.7, the coefficients λ_q of these operators are easily calculated from Feynman diagrams in a given dark matter model.

From quarks to nucleons

In order to convert WIMP-quark amplitudes to WIMP-nucleon amplitudes, one needs the values of quark currents inside the nucleon. These can be extracted from

experiment or estimated theoretically. The scalar operator $\langle N|m_q\overline{\psi}_q\psi_q|N\rangle$ characteristic of the SI interaction is interpreted as the contribution of quark q to the nucleon mass, M_N,

$$\langle N|m_q\overline{\psi}_q\psi_q|N\rangle = f_q^N M_N \tag{3.11}$$

where the coefficients f_q^N relate nucleon and quark operators,

$$\lambda_N = \sum_{q=1,6} f_q^N \lambda_q \tag{3.12}$$

Note there is no explicit dependence on the quark mass in the cross section for WIMP nucleon scattering. Indeed the quark mass term gets transformed into a nucleon mass. For heavy quarks, Q, the parameter f_Q^N is induced via gluon exchange with the nucleon, see [25]

$$f_Q^N = \frac{2}{27}\left(1 - \sum_{q\leq 3} f_q^N\right) \tag{3.13}$$

The coefficients f_q^N can be determined using the value of the light quark masses extracted from baryon masses, the ratio of the quantities $B_q = \langle N|\bar{q}q|N\rangle$ for u, d and s quarks and from the value of the pion-nucleon sigma-term. It is the latter that has the largest uncertainty, see for example [26, 27]. Alternatively the coefficients f_q^N can be computed directly in lattice gauge theory. In Table **??** we give three different set of values for the quark coefficients with the last row (from lattice calculations) featuring a much smaller s-quark coefficient. The uncertainty in the value of the quark coefficients results in roughly one order of magnitude variation in the direct detection rate.

TAB. 3.1 – Different values for the quark coefficients in nucleons

f_d^p	f_u^p	f_s^p	f_d^n	f_u^n	f_s^n
0.026	0.020	0.12	0.036	0.014	0.12 [28]
0.033	0.023	0.26	0.042	0.018	0.26 [29]
0.026	0.021	0.05	0.038	0.015	0.05 [30]

Scattering rates on nuclei

To get the rate for direct detection of WIMPs as a function of the recoil energy of the nucleus we must take into account both the finite velocity of WIMPs, and the

nucleus form factor. After integration over the incoming velocities of WIMPs, the distribution of the number of events over the nucleus recoil energy reads

$$\frac{dN^{SI}}{dE} = \frac{2M_{det}t}{\pi}\frac{\rho_0}{m_\chi}F_A^2(q)\left(\lambda_p Z + \lambda_n(A-Z)\right)^2 I(E) \tag{3.14}$$

where ρ_0 is the DM density near the Earth, M_{det} the mass of the detector, t the exposure time, $f(v)$ the velocity distribution and

$$I(E) = \int_{v_{min}(E)}^{\infty}\frac{f(v)}{v}dv \tag{3.15}$$

$$v_{min}(E) = \left(\frac{EM_A}{2\mu_\chi^2}\right)^{1/2} \tag{3.16}$$

The nucleus form factor, $F_A(q)$, is a Fourier transform of the nucleus distribution function, ρ_A

$$F_A(q) = \int e^{-iqx}\rho_A(x)d^3x \tag{3.17}$$

where $q = \sqrt{2EM_A}$ and ρ_A is the Fermi distribution function

$$\rho_A(r) = \frac{c}{1+exp((r-R_A)/a)} \tag{3.18}$$

where c is fixed by the normalization condition, $F_A(0) = 1$. The parameters R_A and a can be extracted from muon scattering data, $R_A = 1.23A^{\frac{1}{3}} - 0.6$ fm for a surface thickness, $a = 0.52$ fm.

3.2.2 Spin dependent interactions for Majorana fermoins

The effective Lagrangian for spin dependent interactions of a Majorana fermion at zero momentum transfer reads

$$\mathcal{L}^{SD} = \xi_N\overline{\psi}_\chi\gamma_5\gamma_\mu\psi_\chi\overline{\psi}_N\gamma_5\gamma^\mu\psi_N \tag{3.19}$$

It leads to the squared amplitude

$$|A_N^{SD}|^2 = 192(\xi_N S_N M_\chi M_N)^2 \tag{3.20}$$

In order to get the amplitudes for nuclei we have to sum spin currents produced by protons and neutrons separately. First note that for interactions at rest, the γ_0 component of the pseudovector current, Eq. 3.19, vanishes. The resulting interaction

$\bar{\psi}\gamma_5\gamma_i\psi$ leads to a three dimensional vector current which is proportional to the angular momentum J.

The WIMP-nucleus squared amplitudes is obtained after a non-trivial summation over spins.

$$|A^{SD}|^2 = 256\frac{J_A+1}{J_A}\left(\xi_p S_p^A + \xi_n S_n^A\right)^2 M_\chi^2 M_A^2 \tag{3.21}$$

where S_N^A are the expectation value of the spin content of the nucleon N in a nucleus with A nucleons. By definition, for protons and neutrons $S_p^p = S_n^n = 0.5$ and $S_p^n = S_n^p = 0$. This reduces to Eq. 3.20 in the special case of the nucleon and leads to the cross section at rest for a point-like nucleus,

$$\sigma_0^{SD} = \frac{\mu_\chi^2}{\pi}\frac{J_A+1}{J_A}\left(\xi_p S_p^A + \xi_n S_n^A\right)^2 \tag{3.22}$$

The quantities S_N^A are obtained from nuclear calculations or from simple nuclear models, such as the odd-group model. Tables for typical nuclei used in DM detection can be found for example in [31, 32].

The matrix elements for WIMP nucleon interactions are as before related to the more fundamental matrix elements for WIMP quarks interactions. The effective operators for quarks are similar to the nucleon operators, Eq. 3.19. The coefficients ξ_q are easily calculated from Feynman diagrams in a given dark matter model.

In converting WIMP-quark amplitudes to WIMP-nucleon amplitudes, the values of quark currents inside the nucleon are required. The axial-vector current $\overline{\psi}_q\gamma_\mu\gamma_5\psi_q$ responsible for spin dependent interactions, counts the total spin of quarks and anti-quarks q in the nucleon. Operators for axial-vector interactions in the nucleon are related to those in quarks,

$$\xi_{N,s} = \sum_{q=u,d,s} \Delta q^N \xi_{q,s} \tag{3.23}$$

with

$$2s_\mu \Delta q^N \;=\; \langle N|\overline{\psi}_q\gamma_\mu\gamma_5\psi_q|N\rangle \tag{3.24}$$

Here s_μ is the nucleon spin and Δq^N are extracted from lepton-proton scattering data. The latest determination of the light quark contributions [33] give

$$\Delta_u^p \;=\; 0.842 \pm 0.012, \quad \Delta_d^p = -0.427 \pm 0.013, \quad \Delta_s^p = -0.085 \pm 0.018 \tag{3.25}$$

These results are obtained in the limit of $SU(3)_F$ symmetry while the neutron quantities are simply obtained by an isospin rotation

$$\Delta_u^n = \Delta_d^p, \quad \Delta_d^n = \Delta_u^p, \quad \Delta_s^n = \Delta_s^p \tag{3.26}$$

Finally, after taking into account the velocity distribution, the event rate for spin dependent interactions reads

$$\frac{dN^{SD}}{dE} = \frac{8M_{det}t}{2J+1}\frac{\rho_0}{M_\chi}(S_{00}(q)a_0^2 + S_{01}(q)a_0a_1 + S_{11}(q)a_1^2)I(E) \tag{3.27}$$

where $a_{0,1} = \xi_p \pm \xi_n$ and $S_{00}(q)$, $S_{11}(q)$, and $S_{00}(q)$ are the nuclear structure functions which take into account both the magnitude of the spin in the nucleon and the spatial distribution of the spin at non-zero momentum transfer. These form factors are calculated from detailed nuclear models [34].

3.2.3 Other types of dark matter

The case of other dark matter candidates such as Dirac fermions, scalars or vectors can be treated similarly. In each case, two operators will contribute to the effective Lagrangian that describe scalar or spin dependent interactions. For example for a Dirac fermion there are two operators that contribute to scalar interactions (as well as two more for spin dependent interactions)

$$\mathcal{L}_F = \lambda_{N,e}\bar{\psi}_\chi\psi_\chi\bar{\psi}_N\psi_N + \lambda_{N,o}\bar{\psi}_\chi\gamma_\mu\psi_\chi\bar{\psi}_N\gamma^\mu\psi_N \tag{3.28}$$

One can then follow the procedure described above to compute the cross section for WIMP scattering on nuclei at rest. When relating the operators for quarks to those for nucleons, a new type of current related to the second operator in Eq. 3.28 needs to be considered. The vector $\overline{\psi}_q\gamma_\mu\psi_q$ current is responsible for the difference between χN and $\overline{\chi}N$ cross sections. The interpretation of this current is very simple it counts the number of quarks minus the number of anti-quarks in the nucleon, that is the the number of valence quarks. This current is the only one that does not suffer from theoretical uncertainties when going from the WIMP- quark interaction to the WIMP-nucleon interaction. Indeed only valence quarks contribute to the vector current so that

$$\lambda_{N,p} = \sum_{q=u,d} f_{V_q}^N \lambda_{q,p} \tag{3.29}$$

with $f_{V_u}^p = 2, f_{V_d}^p = 1, f_{V_u}^n = 1, f_{V_d}^n = 2$.

For a real vector field the Lagrangian for scalar interaction reads

$$\mathcal{L}_V = 2\lambda_N M_\chi A_{\chi_\mu} A_\chi^\mu \bar{\psi}_N\psi_N \tag{3.30}$$

and the quark coefficients that relate the nucleon operator to the quark operator are the same as in the Majorana fermion case.

Velocity distribution of dark matter

As we have seen, the nuclear recoil energy measured in direct detection experiments depends on the WIMP velocity distribution in the rest frame of the detector (3.14,3.27). This in turns depends on the WIMP velocity distribution in the rest frame of the galaxy and the Earth velocity with respect to this frame,

$$\vec{v}_1 = \vec{v}_0 + \vec{v}_{pec} + \vec{v}_e$$

where $v_0 = 220 \pm 20$km/s is the velocity of the local stadard of rest[35] $\vec{v}_{pec} = (10.0, 5.2, 7.2)$km/s is the peculiar velocity of Sun in this system and $\vec{v}_e$ is the Earth velocity in the solar system.

The velocity distribution of DM particles on the Earth is obtained from the DM velocity distribution in the rest frame of the Galaxy, F_{GRF}. Because the mass of Galaxy is finite there is some v_{max} such that $F_{GRF} = 0$ for $|V| > v_{max}$, astronomical observations[36] give the 90% confidence interval

$$498km/s < v_{max} < 608km/s$$

with a median likelihood of $v_{max} = 544km/s$.

There are several models of DM velocity distribution[37], they are correlated with the DM density distribution. The simplest and most widely used model to describe the DM density is the isothermal sphere model. In such a model the DM velocity distribution corresponds to a Maxwellian distribution which leads to

$$f(v) = c\left[exp\left(-\frac{(v-v_1)^2}{v_0^2}\right) - exp\left(-\frac{min(v+v_1, v_{max})^2}{v_0^2}\right)\right] \tag{3.31}$$

where c is fixed by the normalization condition $\int_0^\infty f(v)dv = 1$.

Note that the Earth motion around the Sun leads to a 7% modulation effect of v_1 and in turn to a modulation of the signal in direct detection experiments. A modulation signal at 8σ has been observed by DAMA [22]. Taking into account the uncertainty in the various velocities influences the limit on WIMP nucleon cross sections extracted from various experiments even assuming a Maxwellian distribution. Moreover the DM velocity distribution close to the Sun could be quite different from the Maxwell distribution. For example condensation of cold DM in clumps and streams will lead to a delta-function distribution.

Current limits

The current limits from DM searches are displayed in Fig. 3.4 for both the spin independent and spin dependent part. To easily compare the limits from experiments using different nuclei, each experiment interprets its results in terms of the cross section on protons or neutrons. This involves in particular unfolding the velocity distribution, the velocity distribution is always assumed to be isothermal, the default paramters can vary within the error bars 3.31. The best limit for the spin independent cross section was obtained recently by Xenon100, $\sigma_{\chi p}^{SI} = 7 \times 10^{-9}$pb, this already constrains the parameter space of some of the dark matter models. The limits on the spin dependent corss section are not yet as stringent,

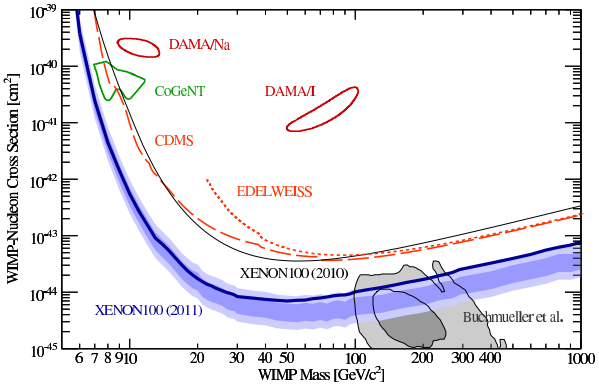

FIG. 3.4 – Results for the spin independent cross section for WIMP scattering on proton as a function of m_χ [38]

3.3 Neutrino from dark matter capture

A WIMP in an orbit passing through a celestial body such as the Sun has a small probability of elastic scattering with nuclei in the celestial body. If the WIMP scatters with a velocity $v < v_{esc}$ it becomes gravitationnally bound. Once captured, WIMPs will scatter from elements in the Sun and settle to the core in a short time. The WIMPs that have accumulated can annihilate with other WIMPs into SM particles. Most of the decay products will be absorbed directly in the core except for energetic neutrinos which can easily pass through the Sun. Neutrinos then travel from the Sun to the Earth, passing through the rock below a detector (or through water in the detector). The neutrino will produce a muon that can be detected in neutrino telescopes such as Kamiokande, Amanda, Antares or IceCUBE. The neutrino induced muons from dark matter annihilation in the Sun can be distinguished

from both the well known atmospheric neutrino flux as well as from solar neutrinos. Indeed their energies are typically $0.3 - 0.5 m_\chi$ much larger than those of solar neutrinos. Neutrino searches therefore have the advantage over other cosmic ray search that the background is well understood.

The differential flux of neutrinos ν_i originating from DM annihilation reads

$$\left(\frac{d\Phi}{dE}\right)_i = \frac{\Gamma_A}{4\pi R^2} \sum_F B_F \left(\frac{dN}{dE}\right)_{F,i} \tag{3.32}$$

where Γ_A is the rate for WIMP annihilation, R is the distance between the source and the detector (Sun-Earth), B_F is the branching fraction for annihilation into a standard final state, F and dN/dE is the differential energy spectrum at the surface of the Sun originating from injection of particles F at the core of the Sun. This spectrum is obtained for example from Pythia.

The number of DM particles, N, in the Sun will increase with the capture rate while their number is depleted by pair annihilations, $\Gamma_A = C_A N^2/2$,

$$\frac{dN}{dt} = C - C_A N^2 \tag{3.33}$$

where C is the capture rate. C_A is related to the annihilation cross section and distribution of WIMPs in the Sun,

$$C_A = \frac{\langle \sigma v \rangle}{V_{eff}} \tag{3.34}$$

where $V_{eff} = 8(m_\chi \rho / 3 m_{Pl}^2 T)^{-3/2}$ is the effective volume of the Sun. Here T is the temperature of the Sun, ρ its core density and $V_{eff} = 0.33 \times 10^{28} (m_\chi / 10 GeV)^{-3/2}$.

The solution for the annihilation rate is

$$\Gamma_A = \frac{1}{2} C_A N^2 = \frac{C}{2} \tanh^2 \sqrt{C C_A} t \tag{3.35}$$

and $\tau = 1/\sqrt{C C_A}$ is the time scale for reaching equilibrium between annihilation and capture. If the age of the solar system ($t_\odot = 4.5 Gyr$) is much greater then τ then equillibrum is reached and the annihilation rate depends only on the capture rate $\Gamma_A = C/2$, otherwise the signal is diluted. It turns out that for typical WIMP annihilation cross section, equilibrium is reached and the signal is full strength.

Capture rate

The capture rate is proportionnal to the number density $n \propto 1/m_\chi$ but the probability of detecting neutrinos is proportionnal to E_ν^2 where a factor of E_ν comes from the

charged current to produce a muon and another factor from the fact that the muon range is proportionnal to E. The neutrino rate increases as m_χ increases contrary to the direct detection rate which goes as $1/m_\chi$ **??**. The capture rate depends on the elastic scattering cross section, for the Sun it is dominated by the SD part due to the hydrogen content. To compute the capture rate one must take into account the distribution of WIMPs. One generally assumes a Maxwell-Boltzmann distribution with velocity dispersion $\bar{v} = 270$ km s^{-1}. Information about the composition of the Sun is also required. Furthermore one must integrate over trajectories of WIMPs through the Sun and over the velocity distribution of WIMPs. Finally form factor suppression must be taken into account. Indeed if DM interacts with nuclei and the momentum transfer is not small as compared with the inverse of nuclear radius , the DM does not see the entire nucleus and the cross-section is form-factor suppressed. The Sun has an escape velocity $v_{esc} = 1156 km/s$ so the scattering process can be hard enough that form factor suppression should be taken into account.

The complete and accurate calculation of the capture rate is given in [40]. For completeness we list the approximate formulas [32]

$$C = c\frac{\rho_\chi/0.3}{m_\chi(\bar{v}/270)}\sum_i F_i(m_\chi)\frac{\sigma_0^i}{10^{-40}\text{cm}^2}f_i\phi_i\frac{S(m_\chi/m_{N_i})}{m_{N_i}} \tag{3.36}$$

where $c = 4.8 \times 10^{24}$ s^{-1} for the Sun, m_{N_i} and m_χ, the mass of the nuclear specie and the mass of the DM are given in GeV. $F_i(m_\chi)$ is the form factor suppresssion in the Sun, f_i is the mass fraction of element i, ϕ_i describes the distribution of element i, see Table 8 and 9 in [32].

In the capture rate all dependence on the particle physics model is included in the coefficients λ_p, λ_n that are contained in the elastic scattering cross section, σ_0^i.

Neutrino spectra and muon flux

A precise computation of the neutrino spectra dN/dE requires including hadronization, neutrino absorption and stopping of heavy hadrons. These effect can lead to an order of magnitude difference in the predicted event rate. Neutrinos injected in the core of the Sun will lose energy via neutral current interactions with the Solar medium and they will be absorbed via charged current interactions ($\bar{\nu}N \to \bar{l}X$) as they pass through the Sun. Thus neutrinos injected with an energy E will leave the Sun with an energy $E_f = E/(1 + E\tau_i)$ with a probability

$$P_f = \left(\frac{1}{1 + E_{\tau_i}}\right)_i^\alpha \tag{3.37}$$

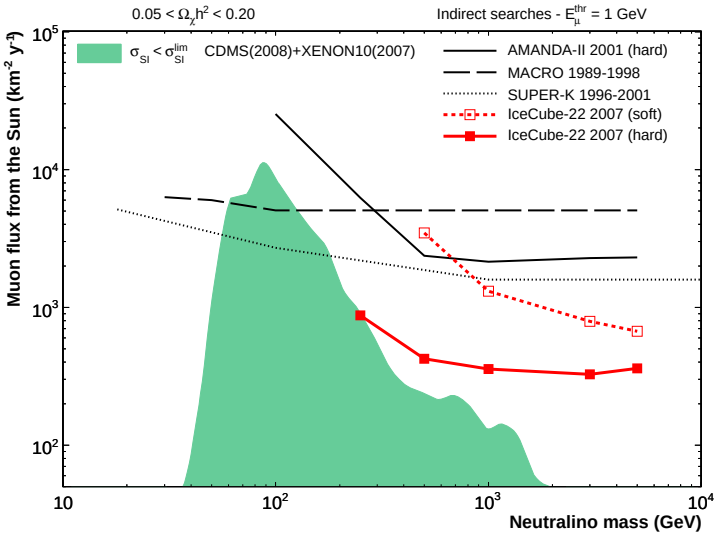

FIG. 3.5 – Limits on muon flux from the Sun as observed by neutrino telescopes [41], the predictions of the constrained MSSM are also displayed.

where $\alpha_\nu = 5.1, \alpha_{\bar{\nu}} = 9$, and the lifetimes $\tau_\nu = 1.01 \times 10^{-3}\text{GeV}^{-1}$ and $\tau_{\bar{\nu}} = 3.8 \times 10^{-4}\text{GeV}^{-1}$. Note that stopping and absorption are different for neutrinos and antineutrinos and therefore lead to different spectra. Finally oscillation effects should be taken into account as well as τ regeneration. Indeed τ will be produced by charged current and will then decay to other neutrinos, $\tau \to X\nu_\tau, e^-\bar{\nu}_e\nu_\tau, \mu^-\bar{\nu}_\mu\nu_\tau$. Typically the neutrino spectrum from DM annihilation into τ or gauge boson pairs will be harder than the one for annihilation into quarks, as seen for example in Fig. **??** that shows the neutrino spectrum at the Earth [42]

Neutrino telescopes observe the muon flux originating from muon neutrinos produced by DM annihilation. The neutrino-induced muon flux is detected by measuring the upward muon produced by a charged-current interaction in the rock below the detector

$$N_\mu = \int V_{eff}(E_\nu)\rho N_A \sigma_{\nu N}^{CC} \frac{dN_\nu}{dE_\nu} dE_\nu \tag{3.38}$$

where V_{eff} is the effective volume of the detecctor and $\sigma_{\nu N}^{CC}$ the charged current neutrino-nucleon cross section. Neutrino conversion can also occur within the detector volume, this is the case for example in large volume detectors such as Antares or IceCUBE. The limit on the muon flux from the Sun from different detectors as a function of the neutralino mass is summarised in Fig. 3.5 with the best limits originating from ICECUBE. These limits are compared with the predictions of the CMSSM and are shown to exclude the upper range of predicted fluxes. [41].

Conclusion

The various dark matter search techniques allows to probe both the spin independent and dependent interactions of dark matter particles with different nuclei as well as the annihilation properties of dark matter. The former is achieved in direct searches and with neutrino telescopes while the latter through the measurement of the flux of photons or charged cosmic rays in indirect searches. These search techniques are reaching a level of snesitivity where meaningful tests of the theoretical predictions of dark matter models (see next chapter) can be achieved. Furthermore they are complementary to each other. The observation of a signal in more than one experiment would allow important cross checks and would also probe the nature of dark matter. We will see in the next chapter how the predictions for different channels can vary depending on the properties of the dark matter candidate. Note however that the interpretation of limits or signals still suffers from large theoretical uncertainties. These range from uncertainties in the quark coefficient in nucleons or in the density and velocity distribution of DM that have an impact on direct detection rates, to the propagation parameters and the presence of astrophysical sources that impact charged cosmic rays including uncertainties in the DM distribution in the center of galaxies that affects photon signals.

Chapitre 4

Dark matter candidates

A variety of dark matter candidates have been proposed, these include both baryonic and non-baryonic candidates. With the exception of the neutrino, most of the non-baryonic candidates consist of yet undiscovered particles. For example the weakly interacting massive particles that we have discussed in previous chapters are predicted in different extensions of the standard model, often the motivations for such extensions are not related to the dark matter problem.. The prime example is the neutralino in supersymmetry.

Before discussing specific candidates, a few comments are in order. Dark matter can be classified into hot, warm and cold according to its velocity, cold DM is non relativistic ($v \approx 0.1c$), warm DM is relativistic ($0.1c < v < 0.95c$) while hot DM is ultra relativistic ($v > 0.95c$). Warm or hot dark matter cannot explain how individual galaxies form. The argument is very simple they move too quickly to be bound to galaxies, thus they cannot explain galactic rotation curve. Furthermore they move too quickly to stay together to form the large scale structure that are observed from weak gravitational lenses (galaxy clusters). Finally the tiny temperature fluctuations in the CMB indicates that matter has clumped together on very small scales, these clumps then grew to form the huge galactic clusters seen today in the Universe. Fast moving particles cannot clump together on small scales furthermore they even prevent the clumping of other matter. This does not mean that warm or hot dark matter cannot exist but only that they cannot be all of the dark matter, cold dark matter will still be needed for galaxy formation.

4.1 Baryonic matter

Massive compact halo objects (MACHO) include very low mass stars with mass $m < 0.08M_{\odot}$, the mass necessary to start nuclear burning. There is no strong motivation for having a large fraction of MACHOs in the halo, nevertheless a better understanding of star formation would be needed to completely rule out this hypothesis. The MACHO hypothesis si however testable by using gravitational microlensing. The MACHO, EROS and OGLE collaborations have searched for such objects by monitoring the luminosity of millions of stars on the Large and Small Magellanic Clouds (LMC) for several years. Examining the intensity as a function of time it is possible to determine the presence of dark objects in our halo as it is expected that during a lensing event a star in the LMC will have its intensity rise over a time period. Such microlensing events were found but lead to estimates that the amount of MACHOS is typically small. For example EROS concluded that MACHO's cannot contribute more than 8% to the mass of the galactic halo while MACHO observed a signal at $0.4M_{\odot}$ with an upper limit at 40% of the mass of the galactic halo.

Other baryonic dark matter candidates include for example remnants of stars, in all cases though there is a need for non-baryonic dark matter.

4.2 Neutrinos

Of the many particles proposed as dark matter the neutrinos have the definite advantage of having been already discovered. As early as 1970 they were the favourite dark matter particle.

In the early Universe neutrinos were kept in thermal equilibrium by their weak interactions with electrons and positrons. The thermally averaged cross section for $T \ll m_W$,

$$\langle \sigma v \rangle \propto g^4 T^2 / m_W^4 \tag{4.1}$$

Their number density is $n \propto T^3$ and their density $\rho \propto T^4$, Eq. 2.34 Neutrinos will be in equilibrium if the interaction rate $\Gamma > H$ where $\Gamma = n\langle \sigma v \rangle$ and H is specified by the Freedmann equation **??**. Substituting the value for H and Γ the temperature for equilibrium is

$$T^3 > \sqrt{\frac{8\pi^3 N}{90}} \frac{m_W^4}{g^2 M_P} \tag{4.2}$$

where $M_P = 1.22 \times 10^{19}$ is the Planck mass. Taking into account photons, electrons, positrons and three neutrino flavours gives $N = 43/4$ so that equilibrium

is maintained at temperatures greater than 1 MeV. This means that neutrinos of $m_\nu > 1MeV$ will begin to annihilate before decoupling and while in thermal equilibrium their number density will be suppressed. Lighter neutrinos however decouple as radiation and therefore do not have the large suppression due to annihilation. The calculation of the number density of light or heavy neutrinos are therefore completely different. For heavy neutrino it is similar to the case of the WIMPs described previously.

Light neutrinos

Light neutrinos are hot (relativistic) dark matter particles. The freeze-out occurs when the neutrinos are relativistic and Y_{EQ} is constant, the asymptotic value of Y, (Y_∞) is insensitive to the precise value of x_f and is given by the equilibrium value at freeze-out, $Y_{EQ} = n/s$ where the number density of relativistic particles is Eq. 2.5

$$n = \frac{\zeta(3)}{\pi^2} g_{eff} T^3 \tag{4.3}$$

where $g_{eff} = g$ for bosons and $g_{eff} = 3/4g$ for fermions and the entropy is given in Eq. 2.34 so that

$$Y_{EQ} = \frac{n}{s} = \frac{45\zeta(3)}{2\pi^4} \frac{g_{eff}}{h_{eff}} \approx 0.278 \frac{g_{eff}}{h_{eff}} \tag{4.4}$$

which lead to a relic abundance (Eq.2.45)

$$\Omega h^2 = 7.65 \times 10^{-2} \left(\frac{m}{eV}\right) \frac{g_{eff}}{h_{eff}} \tag{4.5}$$

since $h_{eff} = 10.75$ and $g_{eff} = 1.5$ for each neutrino specie, the neutrino relic abundance is

$$\Omega_\nu h^2 = \frac{\sum_i m_{\nu_i}}{94eV} \tag{4.6}$$

The best limit on the neutrino masses are obtained from oscillation experiments which have measured a very small difference between neutrino flavours, with mass differences $\Delta m^2 = 10^{-5} eV^2$ for solar neutrinos and $\Delta m^2 = 10^{-3} eV^2$ for atmospheric neutrinos. Furthermore a direct limit on electron neutrino $(2eV)$ is obtained from measuring the end point in the decay $H^3 \to H + e + \nu$. This direct limit combined with the limits on mass differences lead to an upper bound the sum of neutrino masses $\sum_i m_{\nu_i} < 6$eV and to $\Omega h^2 < 0.063$ so that neutrinos alone cannot reproduce the value $\Omega h^2 = 0.11$ of WMAP. In fact observational limits from cosmology allow to constrain the allowed amount of hot dark matter, this provides a limit of 0.63eV

on the sum of neutrino masses (an even better limit can be obtained by modelisation of the Lyman-α forest [43]). Taking the value $m_\nu < 0.6$eV means that neutrinos can form less than 10% of dark matter.

Heavy neutrinos

The computation of the relic density of neutrinos heavier than 1 MeV follows the procedure used for WIMPs, their abundance is strongly reduced by annihilation before they decouple. Their annihilation cross section, which is determined by Z exchange, is proportionnal to m_ν^2/m_Z^4 and since $\Omega h^2 \propto 1/\langle\sigma v\rangle \propto 1/m_\nu^2$, the upper bound on the relic density leads to a lower bound on the neutrino masses of a few GeV. This cannot correspond to the SM neutrinos whose mass is much smaller. Furthermore LEP has excluded new neutrinos that contribute to the invisble width of the Z thus excluding neutrinos with standard model couplings below 45 GeV. New neutrinos heavy enough to escape the LEP bound would only contribute a small amount to the total relic density. Thus both light and heavy neutrinos cannot be the main component of dark matter candidate.

Sterile neutrinos could be a viable alternative. Indeed these particles couple to standard model particles only through their mixing with ordinary neutrinos, their interaction rate is therefore much smaller than that of standard neutrinos. Such sterile neutrinos with a mass below 10keV are suitable dark matter candidates [44] provide they have a very small mixing with ordinary neutrinos. Note that a sterile neutrino in that mass range would be a warm dark matter candidate.

4.3 Axions

The axion is one of the early candidates for dark matter and also one of the better motivated candidate. The axion was introduced to solve the strong CP problem in particle physics. The QCD Lagrangian contains a term

$$\theta \frac{g^2}{32\pi^2} G\tilde{G} \tag{4.7}$$

which violates C and P (in fact QCD depends on θ only through the combination $\bar{\theta} = \theta - arg(m_1, m_2...)$ where m_i are the quark masses. The absence of P and CP violation, for example as measured precisely in the neutron dipole moment, puts a limit on $\bar{\theta} < 10^{-9}$. Naturally one expects this parameter to be $\mathcal{O}(1)$, the smallness of this parameter is the strong CP problem. One solution was proposed by Roberto Peccei

and Helen Quinn, the idea was to render the strong CP violating phase dynamical by introducing a global symmetry, $U(1)_{\rm PQ}$. This symmetry is spontaneously broken and the Goldstone boson of this broken global symmetry is the axion. The axion gets a non-zero mass from the QCD anomaly.

The axion phenomenology is determined by only one parameter f_a, the axion decay constant that determines the scale of symmetry breaking. Its mass

$$m_a = 0.62eV \left(\frac{10^7 \text{GeV}}{f_a}\right) \tag{4.8}$$

and all axion couplings are inversely proportionnal to f_a. In particular the axion couplings to two photons is relevant for laboratory searches. Axion searches are performed by looking for $a \to \gamma$ conversion in a strong magnetic field. This conversion takes place because of a loop-induced $a\gamma\gamma$ coupling

$$\mathcal{L}_{a\gamma\gamma} = -g_\gamma \frac{\alpha}{\pi} \frac{a(x)}{f_a} \vec{E} \cdot \vec{B} \tag{4.9}$$

where $a(x)$ is the axion field and α the fine structure constant. With a very high scale of symmetry breaking the axion becomes invisible.

The axion is constrained by laboratory searches, by stellar colling and by supernova dynamics [45]. In the range $10^{-5} - 10^{-2}$ eV, axions pass all observational constraints and do not overclose the universe. Such a very light particle couples very weakly to ordinary matter so that it never reached thermal equilibrium. The relic density of axions cannot be computed from the equations presented in Chapter 2, nevertheless there are many sources of axion production that make the axion a viable dark matter candidate, examples include vacuum alignment, emission from cosmic strings, etc... Some new laboratory experiments, for example ADMX and CARRACK, are currently looking for the axion in order to probe most of the allowed mass region.

4.4 WIMPs candidates

There are a host of WIMPs candidates as most extensions of the standard model predict new weakly interacting particles. As long as some symmetry guarantees that the lightest of these new particles is neutral and stable it can be a potential cold dark matter candidate. Here we will consider two WIMPs examples, the much studied neutralino in supersymmetry and a new vector boson in extra dimensional models, for a review and a more extensive lists of dark matter candidates, see [46]. Most of these dark matter candidates occur naturally in extensions of the standard model

that were proposed to resolve one of the problem of the standard model, for example the gauge hierarchy problem.

4.5 Supersymmetry

Supersymmetry is one of the better motivated extensions of the standard model that furthermore proposes a WIMP dark matter candidate. It is in particular motivated by attempts to unify gravity with other interactions in the framework of supergravity or supersting theories. Supersymmetry was first introduced as a symmetry that relates fermions and bosons.

$$Q|Fermion\rangle = |Boson\rangle \quad Q|Boson\rangle = |Fermion\rangle \tag{4.10}$$

The generators of a SuperPoincare algebra obey the (anti-)commutation relations

$$\begin{aligned} \{Q_\alpha, \bar{Q}_{\dot{\alpha}}\} &= 2\sigma^\mu_{\alpha\dot{\alpha}} P_\mu \\ \{Q_\alpha, Q_\alpha\} &= \{\bar{Q}_{\dot{\alpha}}, \bar{Q}_{\dot{\alpha}}\} = 0 \\ [P_\mu, Q_\alpha] &= [P_\mu, \bar{Q}_{\dot{\alpha}}] = 0 \end{aligned} \tag{4.11}$$

where P_μ is the translation generator and $\sigma^\mu = (\mathbf{1}_2, \sigma^i)$, with σ^i the Pauli matrices. Note that two supersymmetric transformations give a translation. The irreductible representations of the supersymmetric algebra, called supermultiplets, contain states that are related by $Q, \dot{Q}$ and differ by spin 1/2.

To construct supersymmetric extensions of the standard model, one uses chiral superfields, which contain scalars and fermions and vector superfields which contain vectors and fermions. To each standard model particle is associated a supersymmetric partner with exactly the same $SU(3) \times SU(2) \times U(1)$ quantum numbers but with a spin that diffes by 1/2. For example each left-(right-)handed quark has a spin-0 scalar partner denoted as $\tilde{f}_L(\tilde{f}_R)$. Partners of the spin-1 gauge boson are spin- 1/2 fermions, the gluinos, winos and bino. If supersymmetry is exact standard particles and their supersymmetric partners have the same mass and all interactions are dictated by supersymmetry.

The Higgs sector

In supersymmetry, the Higgs sector must contain an additional Higgs doublet. This is because it is not possible to use the same scalar field to construct mass terms for

both up-type and down-type fermions, the superpotential reads

$$W = \lambda_u^{ij} \bar{u}_R^i h_u Q_L^j + \lambda_d^{ij} \bar{d}_R^i h_d Q_L^j + \lambda_d^{ij} \bar{e}_R^i h_1 L_L^j \tag{4.12}$$

where h_d is similar to the standard model scalar field and h_u is the new field that gives masses to up-type fermions. [1] With two Higgs doublet, the physical states consist of 3 neutral Higgses (two scalars and one pseudoscalar) and of a pair of charged Higgs, $H^{\pm}$. The 3 other degrees of freedom of the complex doublets are the Goldstone bosons that generate masses of gauge bosons. The Higgs doublets have spin 1/2 supersymmetric partners, the higgsinos. The charged higgsinos mix with the winos to form charginos while the neutral higgsinos mixed with the wino and bino to form the neutralinos.

Supersymmetry has the advantage of stabilizing the mass of the Higgs in the standard model. Indeed in the SM, the Higgs mass receives quadratically divergent corrections from quark loops . For example the top quark gives a contribution of the form

$$\delta m_h^2 = 2N_c h_t^2 \int \frac{d^4k}{(2\pi)^4} Tr\left(\frac{i}{k - m_t}\frac{i}{k - m_t}\right) \propto -N_c \frac{h_t^2}{4\pi^2}\Lambda^2 \tag{4.13}$$

where $N_c = 3$ is the color number and $h_t = m_t/v$ is the Yukawa coupling. In supersymmetry the scalar partners of the top quarks also give a contribution to the mass, each of the form

$$\delta m_h^2 = 2\lambda N_c \int \frac{d^4k}{(2\pi)^4}\frac{i}{k^2 - m_{\tilde{t}}^2} \propto \lambda_i N_c \frac{\Lambda^2}{8\pi^2} \tag{4.14}$$

When supersymmetry is an exact symmetry, $\lambda_1 = \lambda_2 = h_t^2$ and $m_{\tilde{t}} = m_t$ so that the scalar partner contribution exactly cancel that of the top quark. Exact supersymmetry would imply that the mass of each supersymmetric particle is equal to that of its standard model partner, this is certainly not the case as we have not discovered any supersymmetric particle yet. Supersymmetry must therefore be broken. The SUSY breaking has to be done in such a way as to preserve the stable Higgs mass. With soft supersymmetry breaking terms the quadratic divergences still cancel, although one obtains finite contribution to δm_h^2 of the order of the supersymmetry breaking scale. This implies that to preserve the solution to the hierarchy problem the scale of supersymmety breaking must not exceed much 1 TeV.

[1] In the standard model one could use instead ϕ and ϕ^*. Note that the extra scalar field is also needed for anomaly cancellation in triangle diagrams.

Coupling constant

Another interesting consequence of supersymmetry is the unification of the coupling constants at high scale. The gauge couplings constants of the SU(3), SU(2) and U(1) gauge groups run with energy. The energy dependence is governed by renormalization group equations and depends on the particle content of the model. The precise measurements of the coupling constants at the electroweak scale at LEP indicate that it is not possible to unify the three couplings at a common scale if only the SM particles are present. The situation is improved if one imbeds the SM within the minimal supersymmetric standard model (MSSM). Supersymmetry offers the possibility of unification of all interactions at a scale around 10^{16} GeV.

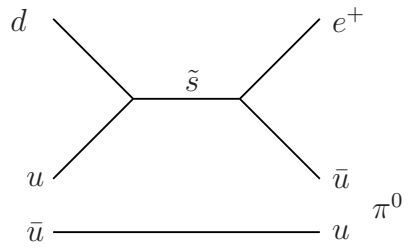

FIG. 4.1 – Example of a supersymmetric diagram that contributes to proton decay.

R-parity and the LSP

In supersymmetry there exist operators that could contribute to proton decay, in particular the one illustrated in Fig. 4.1 where the exchange of a strange quarks induce the decay $p \to e^+\pi^0$. ower limits on the proton lifetime require that these operators be suppressed. If one introcudes a discrete symmetry, R-parity, which is defined as

$$R = (-1)^{3(B-L)+2S}$$

then this interaction cannot take place. All standard particles have $R = +1$ while all their superpartners have $R = -1$. R-parity has an important consequence : a supersymmetric particle cannot decay into two SM particles, this means that the lightest supersymmetric particle will be stable, hence it will be a potential dark matter candidate.

In the general MSSM, the masses of supersymmetric particles are free paramters. The lightest one can therefore be a neutral or a charged particle. Only the first possibility allows for dark matter. The neutral sparticles include the partner of the

neutrino and the neutralino which is a superposition of the supersymmetric partners of the U(1) and SU(2) gauge bosons as well as the Higgs doublets. It turns out that only the neutralino is a good dark amtter candidate, we will examine its properties in more detail below.

4.5.1 The minimal supersymmetric standard model

Without knowing the details of the supersymmetry breaking mechanism one can still write the most general supersymmetric Lagrangian with soft breaking terms. This is called the Minimal Supersymmetric standard model (MSSM), it is minimal because it contains only the particles of the standard model (as well as one additional Higgs doublet) and their supersymmetric partners. When supersymmetry is exact, the Lagrangian is uniquely specified by taking the supersymmetric generalization of the SM Lagrangian with chiral superfields S, ψ (for scalars and fermions) and vector superfields A, λ (for vector fields and their fermionic partners), see the appendix for more details,

$$\mathcal{L} = \mathcal{L}_{gauge} + \mathcal{L}_{kinetic} + \mathcal{L}_{Yukawa} + \mu h_d h_u \tag{4.15}$$

The Lagrangian contains only one new parameter μ. Supersymmetry must however be broken, the most general Lagrangian which violate SUSY without disturbing cancellations of quadratic divergences in scalar masses is called the soft SUSY breaking Lagrangian. It contains the following mass terms,

$$-\mathcal{L}_{gaugino} = \frac{1}{2}\left[M_1 \tilde{B}\tilde{B} + M_2 \sum \tilde{W}^\alpha \tilde{W}_\alpha + M_3 \sum_{\alpha=1}^{8} \tilde{G}^\alpha \tilde{G}_\alpha\right] \tag{4.16}$$

$$-\mathcal{L}_{sfermions} = \sum_{i=1,3}\left(m^2_{\tilde{Q}_i}\tilde{Q}_i^\dagger \tilde{Q}_i + m^2_{\tilde{L}_i}\tilde{L}_i^\dagger \tilde{L}_i + m^2_{\tilde{u}_i}|\tilde{u}_{R_i}|^2 + m^2_{\tilde{d}_i}|\tilde{d}_{R_i}|^2 + m^2_{\tilde{l}_i}|\tilde{l}_{R_i}|^2\right) \tag{4.17}$$

$$-\mathcal{L}_{Higgs} = m^2_{H_u} H_u^\dagger H_u + m^2_{H_d} H_d^\dagger H_d + B\mu(H_u H_d + h.c) \tag{4.18}$$

$$\mathcal{L}_{trilinear} = \sum_{i,j}\left[A_u^{ij} Y_u^{ij} \tilde{u}_{R_i} H_u \tilde{Q}_j + A_d^{ij} Y_d^{ij} \tilde{d}_{R_i} H_d \tilde{Q}_j + A_l^{ij} Y_l^{ij} \tilde{l}_{R_i} H_u \tilde{L}_j\right] \tag{4.19}$$

The scalar potential is the sum of the last three terms.

Requiring electroweak symmetry breaking imposes a condition on the Higgs potential,

$$\begin{aligned} V_{Higgs} &= (m^2_{H_d} + \mu^2) H_d^\dagger H_d + (m^2_{H_d} + \mu^2) H_d^\dagger H_d + B\mu(H_u H_d + h.c.) \\ &+ \frac{g_1^2 + g_2^2}{8}(H_d^\dagger H_d - H_u^\dagger H_u)^2 + \frac{g_2^2}{2}(H_d^\dagger H_u)(H_u^\dagger H_d) \end{aligned} \tag{4.20}$$

Indeed electroweak symmetry breaking requires a negative mass squared terms for some combination of H_u and H_d. The two minimization conditions,

$$\frac{\partial V_{Higgs}}{\partial H_d^0} = \frac{\partial V_{Higgs}}{\partial H_u^0} = 0 \tag{4.21}$$

then give a condition on μ^2 and $B\mu$

$$\begin{aligned} \mu^2 &= \frac{1}{2}\left[\tan 2\beta \left(m_{H_u}^2 \tan\beta - m_{H_u}^2 \cot\beta\right) - M_Z^2\right] \\ B\mu &= \frac{1}{2}\sin 2\beta \left[m_{H_u}^2 + m_{H_d}^2 + 2\mu^2\right] \end{aligned} \tag{4.22}$$

The physical Higgs masses are then easily extracted

$$\begin{aligned} m_A^2 &= -B\mu/\sin\beta\cos\beta \\ m_{H^+}^2 &= m_A^2 + m_W^2 \\ m_{h,H}^2 &= \frac{1}{2}\left(m_A^2 + m_Z^2 \mp \sqrt{(m_A^2+m_Z^2)^2 - 4m_Z^2 m_A^2 \cos^2 2\beta}\right) \end{aligned} \tag{4.23}$$

From this one gets an upper bound on the lighter Higgs mass,

$$m_h^2 < \cos^2 2\beta M_Z^2 \tag{4.24}$$

where $\tan\beta = v_1/v_2$ is the ratio of the vevs. This prediction contradicts the limits on the Higgs obtained at LEP ($m_h > 114$GeV). However this does not mean that supersymmetry is not correct, indeed large radiative corrections, in particular those due to stop quarks increase the Higgs mass above the Z mass.

$$\Delta m_h^2 = \frac{3}{4\pi^2} v^2 y_t^2 \sin^4\beta \log\left(\frac{m_{\tilde{t}_1} m_{\tilde{t}_2}}{m_t^2}\right) \tag{4.25}$$

Large correctinos to the Higgs mass are found for large values of $\tan\beta$ and for a heavy stop sector.

Free parameters

Allowing for flavour violation, the soft Lagrangian contains more than 100 parameters (more than 200 is phases are allowed), for example each of the soft term in Eq. **??** are 3X3 matrices with 9 real and complex parameters. These parameters can be derived from a few fundamental parameters if the model is enbedded in a unified model defined at the GUT scale and some mechanism for supersymmetry breaking

is assumed. The soft parameters obey renormalization group equations which determine their behaviour as a function of energy. The spectrum of superparticles at the weak scale can thus be predicted from a restricted sets of parameters. The GUT scale models include those where supersymmetry is broken by supergravity, for example the much studied CMSSM which has only 4 1/2 free parameters, anomaly-mediated symmetry breaking models, gauge mediated symmetry breaking models as well as a host of string inspired models.

Without going to a complete model define at the GUT scale, one can still work within the context of the MSSM with a manageable number of parameters by making a few simple assumptions :

– All parameters are real - that is there is no new source of CP violation
– All mass matrices and trilinear couplings are flavour diagonal
– The first and second generation of sfermions are identical

While there is no real justification for the first assumption, the second assumption is motivated by the fact that non diagonality in the mass matrices induces some flavour changing neutral current which are known to be suppressed. Likewise the third assumption is motivated by experimental results, resulting from non observation of rare processes in the Kaon and lepton sector. This leaves 22 free parameters in the MSSM :

– $\tan\beta$: the ratio of the vevs of the two Higgs doublet fields
– m_{h_u}, m_{h_d} : the Higgs mass parameters squared
– M_1, M_2, M_3 the bino wino and gluino masses
– $m_{\tilde{Q}}, m_{\tilde{u}_R}, m_{\tilde{d}_R}, m_{\tilde{L}}, m_{\tilde{e}_R}$: the first and second generation sfermion masses
– $m_{\tilde{Q}_3}, m_{\tilde{t}_R}, m_{\tilde{b}_R}, m_{\tilde{L}_3}, m_{\tilde{\tau}_R}$ the third generation sfermion masses
– A_u, A_d, A_e : the first and second generation trilinear couplings
– A_t, A_b, A_τ : the third generation trilinear couplings

One can trade the Higgs mass parameters with the more physical parameters μ and m_A using Eq. 4.22, 4.23.

4.5.2 Properties of the neutralino LSP

The lightest neutralino can be the LSP and therefore a potential dark matter candidate. We must however examine more closely its properties to see if/when it matches the requirement set by the relic density as well as by other dark matter searches. The neutralino is a Majorana particle, meaning that it is its own anti-particle. Although supersymmetry dictates the interactions of the gauginos, sfermions and higgsinos,

the annihilation properties of the neutralino LSP whish is a mixed state, are model dependent.

The neutralino mass matrix

The mass matrix for the neutralinos in the basis $\tilde{B}, \tilde{W}, \tilde{H}_u\tilde{H}_d$ reads

$$M_{\tilde{\chi}^0} = \begin{pmatrix} M_1 & 0 & -M_Z\cos\beta\sin\theta_W & M_Z\sin\beta\sin\theta_W \\ 0 & M_2 & M_Z\cos\beta\cos\theta_W & -M_Z\sin\beta\cos\theta_W \\ -M_Z\cos\beta\sin\theta_W & M_Z\cos\beta\sin\theta_W & 0 & -\mu \\ M_Z\sin\beta\sin\theta_W & M_Z\cos\beta\sin\theta_W & -\mu & 0 \end{pmatrix}. \tag{4.26}$$

This matrix is diagonalized by an unitary transformation

$$M^0_{diag} = N^* M_{\tilde{\chi}^0} N^\dagger \tag{4.27}$$

The mass and nature of the neutralino LSP is determined by the smallest mass parameter. The LSP is bino if $M_1 < M_2, \mu$, wino if $M_2 < M_1, \mu$ and higgsino if $\mu < M_1, M_2$. Since there are two eigenvalues that are determined by μ in the latter case it means that the second neutralino as well as the chargino (see below) are nearly degenerate, $m_{\tilde{\chi}_1} \approx m_{\tilde{\chi}_2} \approx m_{\tilde{\chi}^+}$. The bino/higgsino fraction of the LSP are defined respectively as $f_B = N^2_{11}$, $f_H = N^2_{13} + N^2_{14}$.

The chargino mass matrix

In the $\tilde{W}^+, \tilde{h}^+$ basis, the chargino mass matrix reads,

$$M_{\tilde{\chi}^+} = \begin{pmatrix} M_2 & \sqrt{2}m_W\sin\beta \\ \sqrt{2}m_W\sin\beta & \mu \end{pmatrix}. \tag{4.28}$$

This matrix is diagonalized by a bi-unitary transformation

$$M_{diag} = U M_{\tilde{\chi}^+} V^T \tag{4.29}$$

The lightest chargino is determined by the relative size of μ and M_2. It is constrained by LEP direct searches to be heavier than 103 GeV. This means that $M_2, \mu >$ 100 GeV and therefore imposes some restrictions on the neutralino mass matrix. In particular in the context of the CMSSM where $M_1 = M_2/2$ this poses a lower limit on the neutralino mass of ≈ 50 GeV. There is no such direct limit on the LSP mass if one relaxes the universality between gaugino masses.

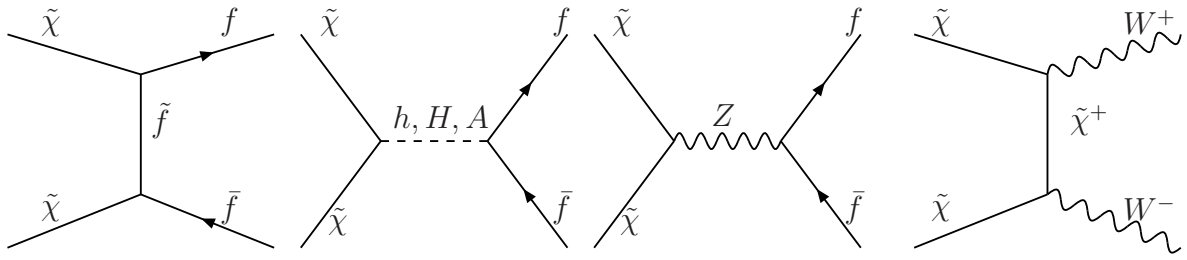

FIG. 4.2 – Some of the diagrams that contribute to annihilation of pairs of Majorana fermions

The sfermions

In the $\tilde{f}_L, \tilde{f}_R$ basis, the sfermion mass matrix reads,

$$m^2_{\tilde{f}} = \begin{pmatrix} m^2_{\tilde{L}} + (I^3_f - Q_f s^2_W) m^2_Z \cos 2\beta + m^2_f & m_f(A_f - \mu \tan\beta^{-2I^3_f}) \\ m_f(A_f - \mu \tan\beta^{-2I^3_f}) & m^2_{\widetilde{f_R}} - Q_f s^2_W m^2_Z \cos 2\beta + m^2_f \end{pmatrix}. \tag{4.30}$$

where $m_{\tilde{L}}, m_{\tilde{R}}$ are the soft masses, Q_f and I^3_f are the charge and isospin of the standard fermion. Note that the left-right mixing (off-diagonal) term is proportionnal to the fermion mass and is typically relevant only for the third generation. Charged fermions are also constrained by LEP direct searches to be generally heavier than 103 GeV. This limit can be relaxed in some scenarios where there are degeneracies between sparticle masses. The Tevatron and the LHC have also derived model dependent limits on sparticle masses, in particular squarks and gluinos. Typical lower bounds on the mass of squarks and gluinos vary from 500-750GeV, these limits are likely to improve in the next few months.

4.5.3 Neutralino as dark matter

The first criteria for the stable neutralino to be a good dark matter candidate is that it satisfies at least the WMAP bound on the relic density. [2] As we have seen before the relic density of a WIMP depends only on the thermally averaged effective annihilation cross section, which include annihilation into all pairs of SM particles as well as in some case coannihilation processes. The parameters that influence neutralino annihilation are its mass and its couplings (these in turn depend whether

[2] If the lower bound is not satisfied it would mean that the neutralino forms only part of the dark matter.

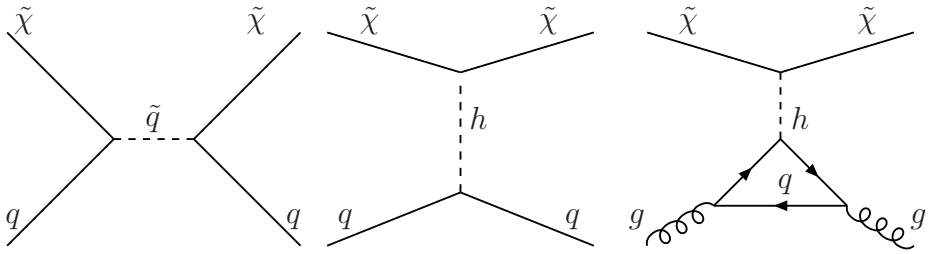

FIG. 4.3 – Diagrams that contribute to spin independent neutralino nocleon interactions in the MSSM.

the neutralino is mostly bino, wino or higgsino), the mass of the sparticles that enter annihilation processes and eventually the mass of the NLSP when coannihilation is relevant. Some of the dominant annihilation processes are displayed in Fig. **??**, we will see below which one typically dominate for different choices of neutralinos. The second criteria for a good dark matter candidate is that limits (or eventually signals) from direct detection must be satisfied. The diagrams that contribute to neutralino scattering on nuclei are displayed in Fig. 4.3,4.4. These diagrams are related to the ones entering annihilation processes except that sfermion exchange is in this case limited to squark through the coupling to quarks in the nucleons. Higgs exchange contribute through its coupling to quarks as well as through loop-induced couplings to gluons. Finally Z exchange gives a contribution to the spin dependent part (the spin independent contribution is suppressed for a Majorana particle). Higgs exchange typically dominate the SD/SI direct detection respectively unless their coupling to the LSP is strongly suppressed. This is because of the mass scale involved. Taking into account the dominant Higgs exchange diagram only, the spin independent interaction reads

$$\lambda_N = -m_N \frac{g^2}{4M_W c_W} \sum_{i=1,2} \sum_q f_q^N \frac{g_{h_i qq} g_{h_i \chi\chi}}{m_{h_i}^2} \tag{4.31}$$

where $h_i = h, H$, $g_{h_i\chi\chi}$ is defined in Appendix A, $g_{huu} = \cos\alpha/\sin\beta$, $g_{hdd} = -\sin\beta/\cos\beta$, $g_{Huu} = \sin\alpha/\sin\beta$, $g_{Hdd} = \cos\alpha/\cos\beta$ and α is the Higgs mixing angle. In the decoupling limit, at large M_H,$\sin\alpha = -\cos\beta$.

Limits from indirect detection should also be satisfied. These also depend on the neutralino annihilation cross section although in this case the velocity involved is much smaller than at freeze-out, $v = 0.001c$. The channels which proceed through p-wave (those with $b >> a$ in $\sigma = a + bv^2$) will be strongly suppressed, in particular neutralino annihilation into fermions at $v \to 0$ is $\propto (m_f/m_\chi)^2$ so is strongly suppressed for light fermions. In this case one can have $\sigma v_{\text{Freeze-out}} << \sigma v|_{v=0}$.

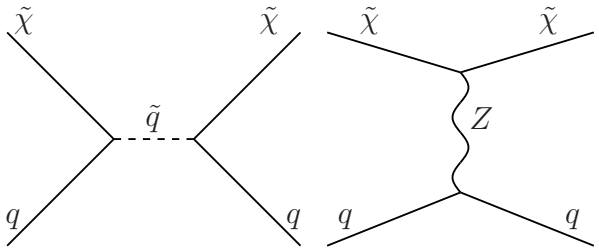

FIG. 4.4 – Diagrams that contribute to spin dependent neutralino nucleon interactions in the MSSM.

Since annihilation of neutralinos into W and Z pairs is not suppressed, typically the preferred annihilation channels are $WW, ZZ, t\bar{t}, b\bar{b}$.

Next we consider different neutralino scenarios and examine its annihilation properties. These depend on the couplings involved in the dominant annihilation processes. For completeness all the couplings of the neutralinos are listed in Appendix A.

The bino

The simplest case is the one of the bino LSP, the bino does not have interactions with the rest of the gauge/gaugino sector so the only relevant couplings are those to the fermion-sfermion, see Tab. 3 in Appendix A. Those are directly proportional to the hypercharge and therefore are largest for the right-handed fermions which have $Y = -2$. The main annihilation channel of the bino LSP is into fermion pairs, through t-channel exchange of a sfermion, Fig. **??**a. The cross section can be easily computed and is proportionnal to $m^2_{\tilde{\chi}}/m^4_{\tilde{R}}$. Therefore it is largest when both the neutralino and the sfermion are light. As an example the variation of Ωh^2 with the sfermion mass for a MSSM scenario with a dominantly bino LSP is displayed in Fig. 4.5. Here the lightest neutralino has a mass $m_\chi = 116$GeV and its bino fraction is 98%. For heavy sleptons the relic density is much above the WMAP preferred value, it decreases with the slepton mass until the mass difference with the LSP is small enough for coannihilation processes to play a role. Then the relic density drops rapidly. For example when the mass difference $m_{\tilde{\chi}} - m_{\tilde{l}} = 10$GeV, $\Omega h^2 = 0.1$ and coannihilation dominates. The main coannihilation processes are $\chi\tilde{l} \to l\gamma$ where $l = e, \mu, \tau$. Typically the channels involving sfermions are more efficient than the ones with only a bino so as long as the Boltzmann suppression factor is not too important, coannihilation can reduce the relic density and bring it in the WMAP range even for neutralinos of several hundred GeV's.

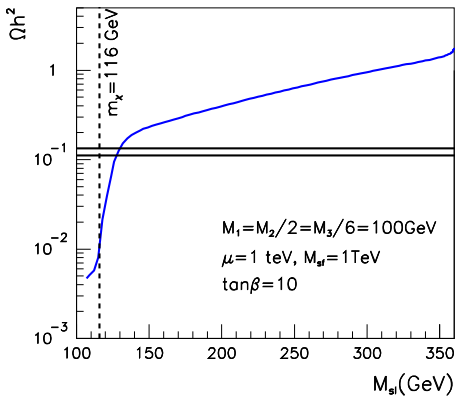

FIG. 4.5 – Ωh^2 as a function of the common RH slepton mass in the MSSM with a bino as the lightest neutralino. The horizontal lines indicate the region preferred by WMAP. The vertical line corresponds to the mass of the lightest neutralino. Here $m_A = 1$ TeV.

In this scenario the direct detection cross section receives a contribution from both squark and Higgs exchange (the latter through the small higgsino component of the LSP) and is therefore not directly related to the annihilation process dominated by slepton exchange. The direct cross section is not large $\sigma^{SI} = 2 \times 10^{-9}$pb and about a factor three below the best exclusion limits of Xenon100, Eq. **??**. when Ωh^2 is reduced by the contribution of coannihilation processes, it is possible to obtain scenarios that are compatible with WMAP yet which feature a much suppressed direct detection cross section.

The indirect detection signatures of the bino scenario can be suppressed as well,this is because the main annihilation process into fermions proceeds through p-wave. At small velocities, one has $\sigma v|_{v\to 0} = 5 \times 10^{-28}\text{cm}^3/\text{sec}$, much below the typical value expected at freeze-out, Eq. **??**. Nota that the NLSP's that were around at freeze-out will have all decayed into the LSP, so only LSP pair annihilation processes contribute to the indirect detection signatures.

The higgsino or bino/higgsino

A higgsino LSP ($f_H \approx 1$) couples also to fermions (with a coupling proportional to the fermion mass) but most importantly it couples to chargino-W pairs as well as to the Z boson. The former coupling means that the higgsino LSP will annihi-

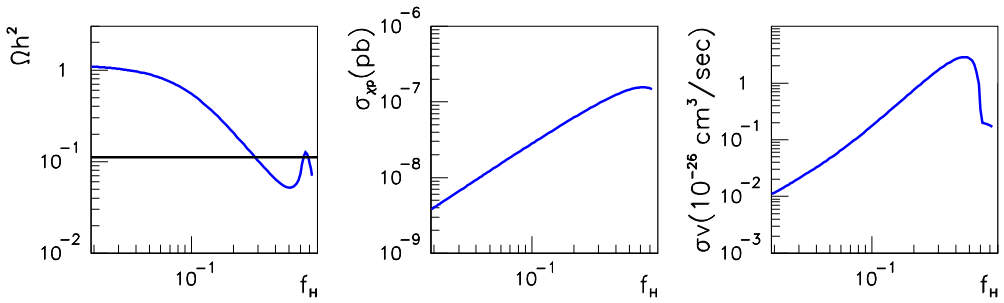

FIG. 4.6 – Ωh^2, $\sigma^{SI}_{\chi p}$, $\sigma v|_{v=0}$ as a function of the higgsino fraction of the LSP in the MSSM with a mixed bino/higgsino as the lightest neutralino. The $M_1 = M_2/2 = 100\text{GeV}, \tan\beta = 10$, $m_A = 1\text{TeV}$ and $m_{\tilde{f}} = 1\text{TeV}$. The horizontal lines indicate the region preferred by WMAP.

late efficiently into W pairs. Furthermore an almost pure Higgsino will lead to nearly degenerate neutralino/chargino NLSP's ($m_{\chi_1} \approx m_{\chi_2} \approx m_{\chi^+} \approx \mu$) and receive important contributions from coannihilation processes. Therefore the dominantly higgsino LSP tends to have a relic density that is below the WMAP range unless it is well above the TeV scale. On the other hand a mixed bino/higgsino LSP has naturally an abundance in the desired range. The strong dependence of the relic abundance on the higgsino fraction is illustrated in Fig. **??**. Note that in this figure, the mass of the LSP is not constant, it varies between $m_\chi = \text{GeV}$ for $\mu = 100 - 400\text{GeV}$.

The scattering of neutralino on nucleons is enhanced in the case where the higgsino fraction is large because the coupling of the light higgs to neutralinos is also large. These scenarios are therefore challenged by recent results from direct dark matter searches. For example, for the parameters that predict a value of the relic density in agreement with WMAP, $\sigma^{SI}_{\chi p}$ lies above the exclusion limit of Xenon and CDMS, see fig. **??**b. In this type of scenario $\sigma v|_{v=0}$ is similar to the value expected at freeze-out since there is no p-wave suppression. This leads to signals that can be large enough to be probe by indirect searches.

The higgsino component of the LSP also opens up the possibility of annihilation through a s-channel Higgs or Z exchange, this process can be strongly enhanced if the masses are such that $m_\chi \approx m_R/2$ where $R = h$ or Z. Indeed the cross section is proportionnal to $1/(s - m_R^2)^2$ with $s \approx 2m_\chi$. Only a small higgsino component is sufficient to decrease significantly Ωh^2 when this condition is fulfilled. This is the only annihilation mechanism that allows to have $\Omega h^2 \approx 0.1$ for a dominantly

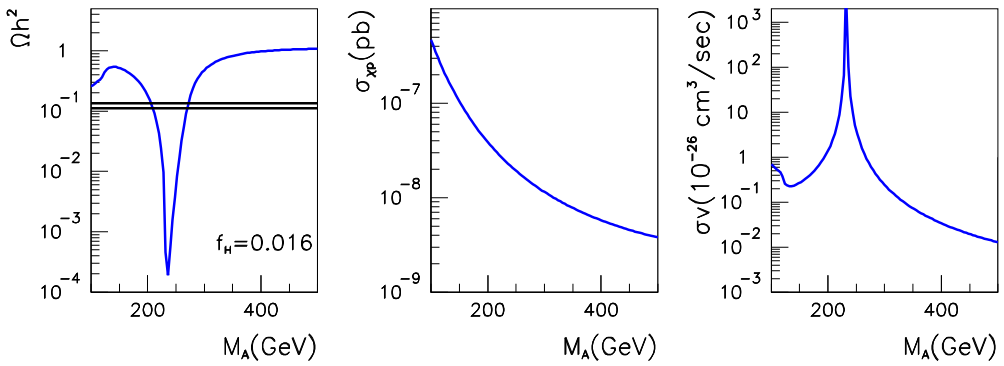

FIG. 4.7 – a) Ωh^2, $\sigma^{SI}_{\chi p}$, $\sigma v|_{v=0}$ as a function of the pseudoscalar mass, m_A in the MSSM in a scenario with $\mu = 420$ GeV, $M_1 = M_2/2 = 100$GeV, $\tan\beta = 10$. For these parameters the LSP is dominantly bino with a higgsino fraction $f_h = 0.016$ and $m_{\tilde{\chi}} =$ GeV. The horizontal lines indicate the region preferred by WMAP.

bino LSP (with small higgsino component) at the TeV scale. The rapid variation of Ωh^2 when the mass of the pseudoscalar Higgs mass is $m_A \approx 2m_\chi$ is displayed in Fig. 4.7a. This resonance effect is also observed for the annihilation cross section at small velocities leading to a strong enhancement of the signal in indirect detection (with $\sigma v \approx 10^{-23}\text{cm}^3/\text{sec}$), Fig.4.7b. On the other hand for direct detection the Higgs is exchanged in t-channel and no resonance effect is expected, see Fig. **??**b. In this scenario, $\sigma^{SI}_{\chi p}$ is above the current limit when m_A is small and drops rapidly with the Higgs mass.

Annihilation of LSP's through a s-channel Higgs exchange can be the dominant process even without a resonance effect. For example the couplings of the heavy Higgs to b-type quarks are enhanced at large values of $\tan\beta$, leading to efficient annihilation of pairs of LSPs into b quarks.

The wino

The wino is not commonly considered to be the LSP because it requires $M_2 << M_1$ which means that in a context of a GUT scale model one must introduce some nonuniversality in the gaugino mass. The wino couples to left-handed fermions as

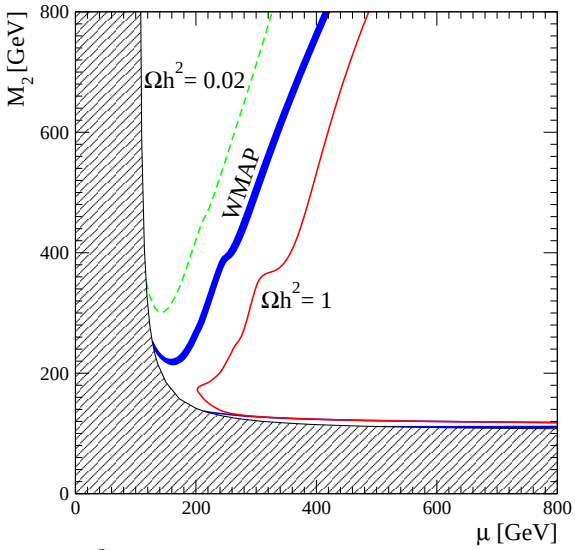

FIG. 4.8 – Contours of Ωh^2 in the $\mu - M_1$ plane in the MSSM in a scenario with heavy sfermions and $m_A = 1$ TeV.

well as to chargino/W, see Tab. **??**. As opposed to the higgsino there is no direct coupling to the Z. The dominant annihilation are into W pairs through t-channel exchange of a chargino or into fermion pairs. For the latter to be efficient one needs light LH sfermions. The pure wino will be nearly degenerate with the chargino therefore coannihilation processes will also come into play. The pure wino does not couple to Higgs so the direct detection rate is much suppressed, a small mixture of higgsino can however lead to rates near/above the present exclusion limit.

4.5.4 Summary

In summary, in the case of heavy sfermions and assuming the gaugino mass relation $M_1 < M_2$, one finds that the WMAP bound is satisfied when $M_1 \approx \mu$ so that the LSP has some higgsino component, see Fig. **??**. The allowed region is a narrow strip in parameter space but there is a large region where the upper bound is satisfied. If in addition some Higgs with a mass $m_h \approx 2m_\chi$ exists, the WMAP upper cound is easily satisfied provided the LSP has some higgsino admixture. Finally light sfermions offer more possibility for annihilation even for a pure bino, note however that sfermion masses are severely constrained by collider limits.

4.5.5 The neutralino LSP in the CMSSM

Now that we have discussed the annihilation properties of the different type of neutralinos we can examine the properties of the neutralino dark matter in a more constrained model where a set of boundary conditions at the unification scale (GUT) are imposed on the fundamental parameters. As an example we will consider the well studied constrained MSSM where the SUSY breaking occurs in a hidden sector and is transmitted to the visible sector through gravitational interactions.

In the CMSSM it is assumed that at some high scale the mass of scalars is universal, m_0, the gauginos have a universal mass $m_{1/2}$ and all trilinear couplings are equal A_0. The ratio of the vev's of the Higgses, $\tan\beta$, is taken as a free parameter, which contrary to the others is defined at the weak scale, the sign of μ is the last free parameter. Note that the value of μ is computed from the symmetry breaking condition. The soft parameters and the particle spectrum at the weak scale are computed from renormalization group equations. The predictions of the CMSSM are that gaugino masses at the electroweak scale are related $M_1 \approx M_2/2 \approx M_3/6$ and that in most of the parameter space the parameter $\mu >> M_1$, this means that the lightest neutralino is usually dominantly bino.One exception is the region at very large values of m_0 , called focus point, where the renormalization group equations are such that the value of the μ parameter drops rapidly when decreasing $m_{1/2}$ eventually reaching a non physical region where $\mu^2 < 0$. Near the non-physical region, we have $\mu \approx M_1$ and the conditions for the mixed bino/Higgsino are satisfied. The exact location of this region depends vey sensitively on the value of the top quark mass, it is favoured by a low m_t. Other predictions for the particle spectrum are that left handed sfermions are heavier than right handed sfermions, and that squarks are heavier that sleptons. This is because the evolution of coloured particle is driven by the strong gauge coupling, that of left-handed leptons by SU(2) coupling while that of right-handed lepton by the U(1) coupling. The LSP is typically the lightest neutralino or the lightest right-handed sfermion,that is $\tilde{\tau}_R$ since the mass of the stau is shifted downwards from that of other sleptons by mixing effects.

Because of the restricted sets of parameters, this model faces several constraints from collider searches for new particles, including the Higgs, as well as from precision measurements, B-physics observables or muon anomalous magnetic moment. These constraints, listed in Table **??**. Although not directly related to the dark matter sector, have an impact on the predictions of the DM properties as will be made explicit below.

Dark matter properties

In this model, the LSP is mostly bino, as we have discussed above this means that both the bino and sfermions need to be light for the relic density to be compatible with WMAP data. In the CMSSM parameter space this corresponds to the region at low $m_0 - m_{1/2}$, the bulk region. The only possibility to extend the WMAP region to heavier binos, thus larger values of $m_{1/2}$, is to make use of coannihilation. At low values of m_0, when the stau is the NLSP and its mass difference with the LSP is around 10GeV, stau coannihilation processes (notably $\chi\tilde{\tau} \rightarrow \tau\gamma$) reduced Ωh^2 to 0.1. This corresponds to the thin line above the theoretically excluded region in Fig. **??**. Finally one can also make use of efficient resonant annihilation of the LSP through a Z or light Higgs exchange, this works only for $m_{\tilde{\chi}} \approx m_h/2$ or $m_Z/2$, see Fig.4.9.

At large values of $\tan\beta$ two new possibilities open up. The first is the so-called Higgs funnel region where the bino LSP annihilates efficiently through s-channel exchange of a heavy Higgs because of a resonance effect and of the enhanced coupling of the heavy Higgs to quarks. Note that this works even though there is only a small higgsino component in the LSP. The second region is the focus point mentionned above where at large values of m_0 the LSP contains a significant higgsino component. The LSP then annihilates efficiently into W pairs or top quark pairs. This region is found more easily at large values of $\tan\beta$ and depends sensitively on the exact value of the top quark mass.

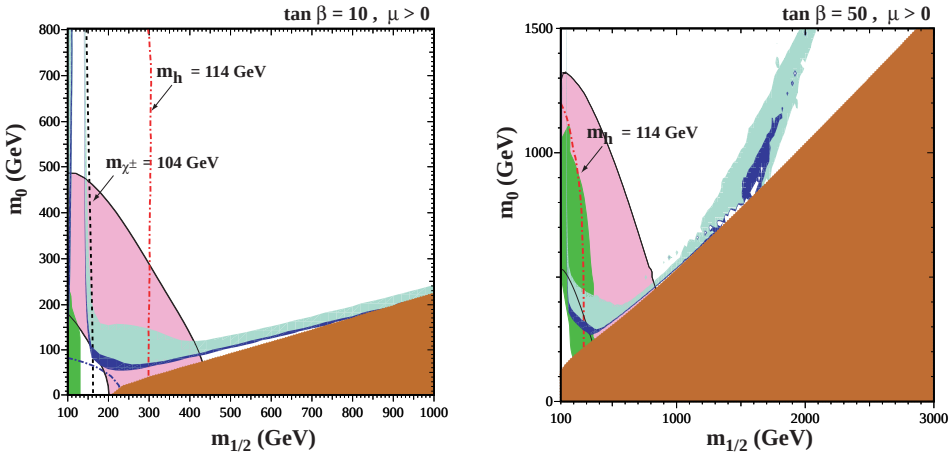

FIG. 4.9 – The parameter space compatible with DM and collider constraints in the $m_0 - m_{1/2}$ plane for a) $\tan\beta = 10$ b)$\tan\beta = 50$ [47].

The expectations for the SI direct detection rate in the CMSSM follow from our discussion in previous sections : the rates are largest either when the bino LSP

is light (in the bulk region) and when the LSP has a large higgsino content (the focus point region). On the other hand much suppressed rates are expected in the coannihilation region, indeed coannihilation is effective in the early universe but only LSP's are left today to scatter with nuclei in a detector. Low detection rate are also expected in the Higgs funnel region, indeed resonance effect works for annihilation but not for scattering off nuclei. For indirect detection, rates are small in the bulk region because the dominant annihilation channel into leptons is suppressed at low velocities. In fact large rates are expected only in the focus point region with a mixed higgsino LSP, while again the coannihilation region is associated with low rates.

The impact of LHC data on these predictions and the complementarity will be summarised next.

Constraints on the MSSM

There exists strong constraints on the parameter space of the CMSSM, direct limits are set by colliders, including LEP, the Tevatron and now the LHC (see next section) and indirect limits occur from loop induced contributions of supersymmetric particles to precision observables or particle masses. Without going into the details of all the various contributions to different processes, one can make a few observations. First the lower limit on the Higgs mass requires large values for the stop masses (hence constrain the low m_0 region) and/or a large value of $\tan\beta$. Second B observables disfavour large contributions from the heavy Higgs exchange that are enhanced at large values of $\tan\beta$, finally the muon $g-2$ favours light sleptons/charginos so as to introduce some deviation from the SM.

These constraints imply that not all of WMAP compatible regions are allowed. First the LEP limit on charginos and neutralinos in this model all but preclude the possibility for annihilation near a Z or light Higgs resonance. Second the limit on the light Higgs mass ($m_h > 114$ GeV) strongly constrains the bulk region especially at low values of $\tan\beta$. The stau coannihilation region is only constrained by the LEP limit on staus. On the other hand, the $g-2$ of the muon favours the light slepton region (low $m_0 - m_{1/2}$) while precision measurements and in particular the W mass (which is subject to radiative corrections from new particles) also favour this region. At large values of $\tan\beta$, B physics observables come into play and disfavour a too light spectrum (the bulk region). This representation of the allowed parameter space in the $m_0 - m_{1/2}$ plane while convenient is a bit misleading because it is done for fixed value of all but 2 parameters. However it is known that the spectrum has a strong dependence on parameters such as m_t. Determining the WMAP allowed regions requires to include uncertainties in all input parameters. Global fits to dark

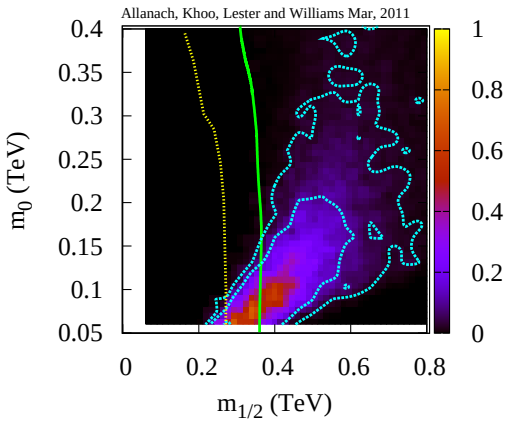

FIG. 4.10 – Global CMSSM fits in the $m_0 - m_{1/2}$ plane : excluding the ATLAS 0-lepton search and The posterior probability of each bin is shown as the background colour, normalised to the maximum bin probability. The region to the left of the almost vertical solid green (dotted yellow) curve is excluded by the ATLAS 0-lepton search (CMS α_T search) at the 95% C.L. The cyan inner (outer) contour shows the 68% (95 %) Bayesian credibility region.

matter and precision observables show that the thin stripped displayed in Fig. **??**a for fixed value of $\tan\beta$ and SM parameters fatten in this case to wide areas. These results show that the favoured region is at low masses although a large fraction of the parameter space is allowed.

LHC and interplay with DM searches

The LHC, a pp collider, has been running at an energy $\sqrt{s} = 7$ TeV and has announced its first limits on the parameters of the CMSSM in the spring of 2011. At the LHC the production of coloured particle, the squarks and gluinos have the largest rate. The signature for these particles are numerous and always include some missing energy for the stable LSP. The signatures are classified according to the number of jets and leptons produced in association with the missing E_T. With a low luminosity, the signatures involving only jets are the most powerful as they provide the best statistics. The results after 35pb^{-1} are presented in Fig. **??**. The bulk region is now severely constrained with limits on squarks and gluinos around 750GeV.

The discovery potential of supersymmetry at the LHC when running at full lumino-

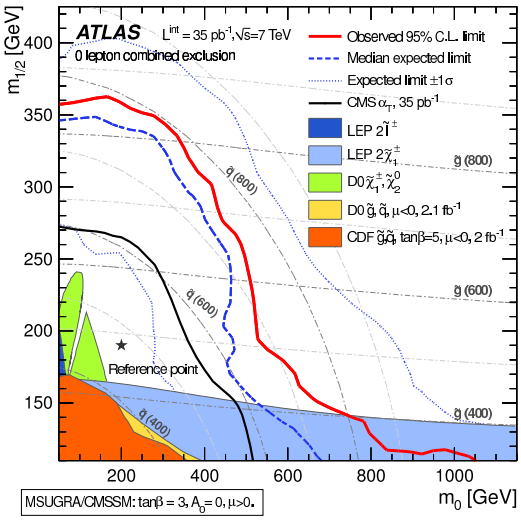

FIG. 4.11 – Exclusion region in the $m_0 - m_{1/2} plane$ of the CMSSM from the ATLAS search for jets and missing energy at $\sqrt{s} = 7$ TeV and $\mathcal{L} = 35\text{fb}^{-1}$.

sity corresponds roughly to gluino masses and squark masses aroudn 2TeV. When projected in the $m_0 - m_{1/2}$ plane this covers a large area of the parameter space although not all the dark matter allowed regions are covered. The bino/light sfermion region will be probed completely soon while part of the coannihilation region/Higgs funnel can be out of reach especially at large values of $\tan\beta$ even with a luminosity of 100fb^{-1}. Furthermore the focus point region can be hard to probe, indeed in this case the squarks are very heavy and the only coloured particle are the gluinos. The reach is therefore much more limited. Direct production of chargino neutralino pair could lead to an observable signature, with trileptons from $\chi^+ \to l\tilde{\nu}\chi_1^0$ and $\tilde{\chi}_2^0 \to \tilde{\chi}_1^0 l\bar{l}$. Searching for this signature allowed Tevatron to put a limit on the chargino mass. . We have seen above that a mixed bino/Higgsino LSP gives large cross section for direct detection. Furthermore the indirect detection rate is not p-wave suppressed. Therefore both these detection modes should easily probe the region thus leading to a nice complementarity between the collider probes of the SUSY parameter space and the DM searches probe of the same parameter space.

Many of the seconclusions are a direct consequence of the relations between the parameters of the model due to the choice of boundary conditions. Changing these conditions by introducing some non-universality in the model can affect the mature of the LSP. For example non-universality in the scalar sector by assuming that $m_{Hu}, m_{Hd} \neq m_0$ at the GUT scale leads to a LSP with a larger higgsino or wino content. As we have discussed above it becomes therefore much easier to satisfy the

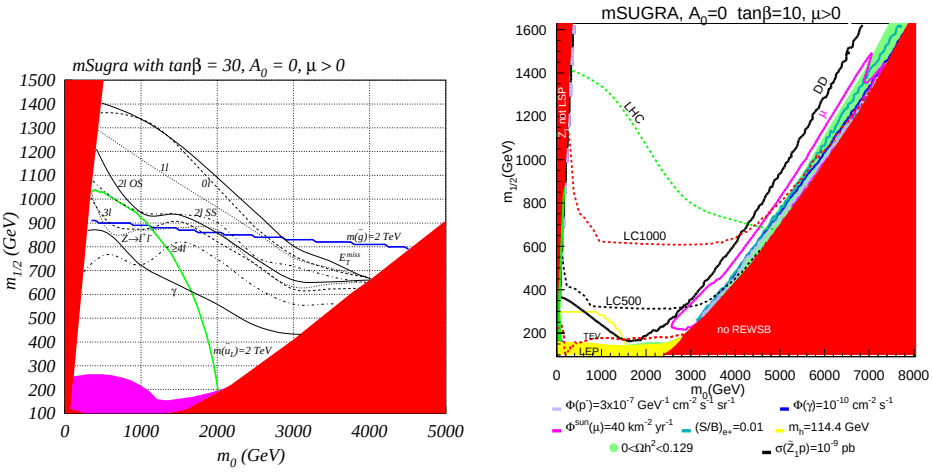

FIG. 4.12 – a) Reach for discovery of supersymmetric particles in the MSSM for the LHC with $\sqrt{s} = 14TeV$ and $\mathcal{L} = 100\text{fb}^{-1}$ b) Interplay of colliders and of direct and indirect detection searches for probing the parameter space of the CMSSM.

upper bound on the relic density and to get a large direct detection cross section [48].

4.5.6 Sneutrino

Although neutral and weakly interacting the sneutrino turns out not to be a good dark matter candidate. The main reason is that its interation with a nucleon is too strong. Indeed the left-handed sneutrino couples to the Z, in the case of a scalar field that is not self-conjugate, the Z exchange contributes to the spin independent sneutrino quark scattering. The cross section can easily be computed,

$$\sigma_{\tilde{\nu}N} = \frac{8G_F^2}{\pi}\mu_{\chi N}^2 |C_N|^2 \tag{4.32}$$

where $\mu_{\chi N}$ is the reduced mass of the nucleon and $C_p = 1/2 - 2s_W^2$, $C_n = -1/2$. This gives a cross section of the order of $\sigma \approx 10^{-2}$ pb for a 100GeV sneutrino whereas the best limit from is $\sigma_{\chi p} = 7 \times 10^{-9}$ pb.

The right-handed sneutrino offers an alternative candidate. This particle is well motivated since it is natural to add a right-handed neutrino to the standard model(and its supersymmetric partner in SUSY extensions) to describe neutrino masses and the observed neutrino oscillations. Since the RH sneutrino does not couple to the Z, the direct detection rate is naturally suprressed. However a pure RH sneutrino cannot

be brought in thermal equilibrium as it does not couple to SM particles. One must appeal to non-thermal processes to make it a good dark matter candidate. On the other hand, thermal sneutrinos can be found in extensions of the MSSM where one introduce some coupling to the Z or Higgs through mixing with the LH sneutrino or through new gauge interactions.

4.5.7 Kaluza-Klein particles

Models with extra dimensions offer the possibility of building a consistent theory of quantum gravity and unification of all interactions. This category of models propose also a solution to the hierarchy problem by effectively lowering the Planck scale after compactification of the extra dimensions on circles of radius R. In a class of models, called universal dimension models (UED), all fields propagate in flat compact dimensions of size $10^{-18}m$. The minimal UED model has only one extra dimension compactified on an S^1/Z_2 orbifold of radius R.Each of the standard model field is accompanied by a tower of KK state, at tree level the nth KK mode has a mass

$$m^n = \sqrt{(n/R)^2 + m^2} \tag{4.33}$$

where m is the mass of the corresponding SM particle. It is therefore natural to expect a rather degenerate spectrum of new particles. These models have the nice feature that they could explain 3 families from anomaly cancellation, could realize dynamical symmetry breaking and predict a long enough decay time for the proton. In some models, a conserved KK parity, $KK = (-1)^n$, ensures that the lightest particle at the first level, the LKP, is stable thus a possible dark matter candidate.

The near degeneracy among KK states is lifted by radiative corrections and the size of these corrections are proportionnal to the SM coupling constants. It is therefore quite natural to have the partner of the U(1) gauge boson B^1 as the lightest KK particle. A typical mass spectrum for $R^{-1} = 500$ GeV is displayed in Fig. The relic density of B^1 is computed by solving the Boltzmann equation as described in Chapter 2. As for other WIMPs it is inversely proportioannal to the annihilatinon cross section. The annihilation of the LKP which is a gauge boson is typically more efficient than that of neutralinos. One particular feature of the model is that annihilation into light fermions is large and not suppressed at small velocities, $\sigma v \approx 95 g_1^4/324\pi m_{B^1}^2$. Both in the early universe and in the galaxy, the dominant annihilation channels is into leptons, with nearly 60% branching ratios. This feature implies a poteltial large signal in positrons. In this class of models one tends to have typically a value for Ωh^2 that is too low unless the LKP mass is in the TeV range.

Another characteristic of the model is the small mass splitting between particles at

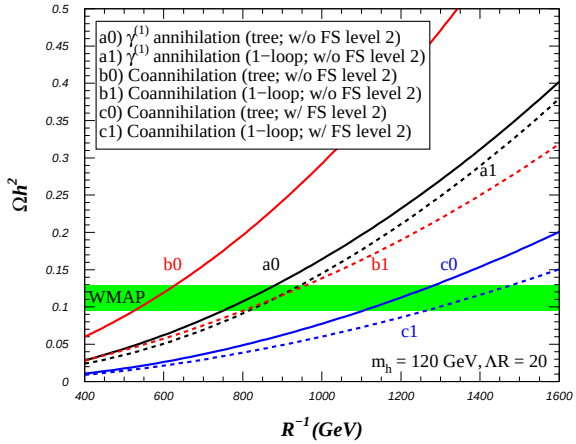

FIG. 4.13 – Ωh^2 vs the scale R^{-1} in minimal UED model with $m_h = 120$ GeV including either only annihilation channels or coannihilation channels with and without level 2 particles in the final state.

a given level which makes coannihilation very natural. Coannihilation channels with leptons have typically smaller cross sections than B^1 annihilation so adding coannihilation channels tend to increase Ωh^2, see Fig. 4.13. The coannihilation channel can however be strongly enhanced by the exchange near resonance of a level 2 particle in the s-channel (the enhancement factor depends on the exact mass of the level 2 particle), in this case the contribution of coannihilation channels is increased and the WMAP compatible region is pushed above the TeV scale.

Dark matter detection

There are three types of diagrams that contribute to elastic scattering of B^1, the exchange of KK -quarks in the s and t channels and of a Higgs boson in the t channel, see fig. **??**. The amplitude for $B^1 q \to B^1 q$ scattering can be computed from the Feynman diagrams, in terms of the effective Lagrangian for the scalar interaction for vector fields, Eq. 3.30

$$\lambda_N = \frac{m_N}{8 m_{B^1}} \sum_q \left(\frac{g_1^2}{m_h^2} + 2 g_1^2 (Y_{q_L}^2 + Y_{q_R}^2) \frac{m_{B^1}^2 + m_{q^1}^2}{(m_{B^1}^2 - m_{q^1}^2)^2} \right) f_q^N \qquad (4.34)$$

where Y_{q_L}, Y_{q_R} are the hypercharge of KK quarks (same as standard quarks) and g_1 is the U(1) gauge coupling. The quark exchange contribution is inversely proportional to the mass splitting between KK-quarks and B^1, For the typical mass difference in the MUED model, $\Delta = m_{q^1} - m_{B^1} \approx 0.17 m_{B^1}$ the amplitude is dominated by Higgs exchange and the cross section is typically quite low, $\sigma^S I_{\chi p} \approx 10^{-10}$pb for $m_{B^1} \approx$

1 TeV. However in non minimal models where masses receive additional corrections, the mass splitting could be much smaller leading to a strong enhancement of the cross section to a level near the present exclusion limit.

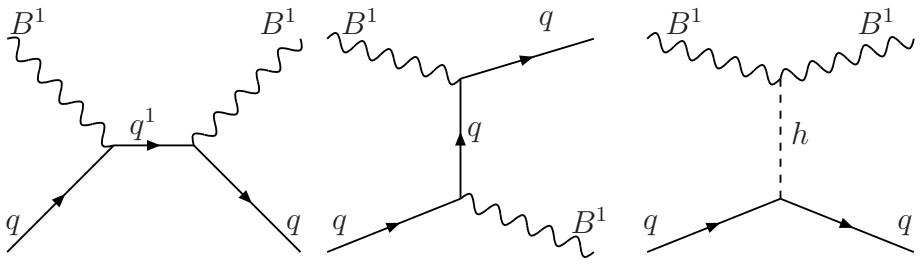

FIG. 4.14 – Diagrams that contribute to spin independent $B^1 - q$ interactions in UED.

The main feature of the UED model is that annihilation into lepton pairs is dominant even at small velocities. This means that the TeV scale B^1 boson is a potential candidate for explaining the PAMELA excess in the positron fraction. Indeed the positron spectrum is expected to be hard in this model [49], however as for other models, the cross section required is much larger than predicted by UED and one therefore needs to appeal to some large boost factor.

The KK particles can be directly produced at colliders, with the largest cross sections expected for coloured particles. The decays of the KK particles are quite similar to those of SUSY particles, with for example $Q^1 \rightarrow Z^1 q$ leading to a signalture of jets with 2 leptons and missing E_T. The mass splitting between KK level particles is small so that jets and leptons are typically softer than in SUSY models, furthermore the spins of the new particles differ by 1/2 from the spin of SUSY particles. The best way to disentangle a new UED signal from a SUSY signal therfore involves spin determination of the new particles. In addition the UED model predicts new particles at the second KK level with masses about twice that of the LKP. Such particles, for example new gauge bosons could be produced on resonance at the LHC.

4.6 SuperWimps dark matter

Super weakly interacting massive particles can also have a relic density in the range determined by WMAP while featuring specific signatures in dark matter searches. In such scenarios dark matter is produced in late decays, WIMPs freeze-out as usual

then each WIMP decay into a superWIMP. Because the superWIMP interactions are very weak they have no impact on the WIMP freeze-out so that WIMPs decouple as usual. Assuming that each WIMP produces one superWIMP the abundance of superWIMP is the same as that of the WIMP and the relic density just scales as the mass ratio

$$\Omega_{SuperW}h^2 = m_{SuperW}/m_{WIMP}\Omega_{WIMP}h^2. \tag{4.35}$$

Note that the decay time of the WIMP can be very long, for example in the case where the superWIMP has only gravitational interactions decay time $\tau = 10^3 - 10^7$s. The abundance of dark matter in superWIMPs scenarios could also result from non-thermal production mechanisms, for example from reheating.

4.6.1 Gravitinos

The gravitino, the spin 3/2 partner of the spin 2 graviton, is a prime example of a superWIMP. It exists in all supersymmetric theories and has been shown to be a good dark matter candidate in gauge mediated SUSY breaking models. In these models the SUSY breaking is transmit from the hidden to the visible sector by loop diagrams with messenger partices $M_{SUSY} = \alpha/(4\pi)\langle F\rangle/M_{mess}$ with $M_{mess} \approx \sqrt{F} = 10^4 - 10^5 GeV$. The gravitino mass is $m_{3/2} = \langle F\rangle/\sqrt{3}M_{Pl}$. The gravitino only interacts through gravitational interactions and is therefore difficult to observe. The mass of the gravitino can be below or above the mass of other supersymmetric particles. In the case where it is the LSP, its relic density can be directly related to that of the NLSP which can be either neutral or charged.

A possible consequence of a gravitino LSP is a new apparently stable charged particle (when the NLSP is charged). The NLSP will have a long lifetime because the decay into a gravitino is mediated by gravitational interaction, the NLSP will therefore decay outside of the detector. It has been suggested to build NLSP traps (large water tanks outside the LHC detectors) to capture these particles and study their decay.

Gravitino dark matter interact so feebly that no signal in direct DM searches is expected. Exotic sgnals might however be found in cosmic rays or with neutrino telescopes. Furthermore because the mechanism that is responsible for the relic density (annihilation) is not the same that the one responsible for source of cosmic rays (decay) the size of the two processes are not correlated and one could even have in principle a much larger signal than expected in indirect detection. This idea was put forward as a possible explanation of the large excess of positrons in PAMELA. In neutrino telescopes one could see the long-lived chardes particles. For example ultra high-energy neutrinos can produce staus via the process $\nu q \to \tilde{\tau}\tilde{q}'$ with the $\tilde{q}'$

eventually decaying into a $\tilde{\tau}$. The long-lived staus can then propagate to neutrino telescopes and leave a signature as two upward-going extremely high-energy charged tracks in neutrino telescopes. Late decays can also leave observable effects on BBN (even improving predictions for light element abundances) or could give distorsion in the spectrum of the CMB (such distorsions have not been observed so far).

4.7 Conclusion

The list of dark matter candidates is rather long even restricting only to the case of WIMPs, we have discussed only a few of the proposed candidates. Understanding the nature of dark matter is therefore an exciting challenge that requires the combined efforts of many different types of searches including both direct and indirect detection as well as collider searches. Colliders are crucial as they offer a better control of the particle physics aspects of the dark matter problem. If new particles are found and missing energy signals observed it will not only narrow down the list of possible extensions of the standard model but also allow to make more precise predictions of cross sections for DM processes within a specific model.

Both DM searches and collider searches are producing lots of new results so that there is high hope that in the next couple of years some dark matter signal will be confirmed.

.1 Appendix A : Interaction of the neutralino in the MSSM

$\tilde{\chi}_i^0 f f$	f_L	f_R
$\tilde{l}_L, \tilde{d}_L$	$I_3 N_{i2} + Y N_{i1} \tan\theta_W$	$\frac{m_f}{M_W \cos\beta} N_{i3}$
$\tilde{u}_L$	$I_3 N_{i2} + Y N_{i1} \tan\theta_W$	$\frac{m_f}{M_W \cos\beta} N_{i4}$
$\tilde{e}_R, \tilde{d}_R$	$\frac{m_f}{M_W \cos\beta} N_{i3}$	$Y N_{i1} \tan\theta_W$
$\tilde{u}_R$	$\frac{m_f}{M_W \cos\beta} N_{i4}$	$Y N_{i1} \tan\theta_W$

Tab. 1 – Neutralino couplings to fermion-sfermions

$\tilde{\chi}_i^0 \tilde{\chi}_i^0 h$	$\frac{e}{s_W c_W} \left(N_{i2} - N_{i1} \tan\theta_W\right) \left(-s_\alpha N_{i3} - c_\alpha N_{i4}\right)$
$\tilde{\chi}_i^0 \tilde{\chi}_i^0 H$	$\frac{e}{s_W c_W} \left(N_{i2} - N_{i1} \tan\theta_W\right) \left(c_\alpha N_{i3} - s_\alpha N_{i4}\right)$
$\tilde{\chi}_i^0 \tilde{\chi}_i^0 A$	$\frac{e}{s_W c_W} \left(N_{i2} - N_{i1} \tan\theta_W\right) \left(s_\beta N_{i3} - c_\beta N_{i4}\right)$
$\tilde{\chi}_i^0 \tilde{\chi}_i^0 Z$	$\frac{e}{2 s_W c_W} \left(N_{i3} N_{i3} - N_{i4} N_{i4}\right) \gamma_\mu \gamma_5$

Tab. 2 – Neutralino coupling to Higgs and Z

	$\gamma_\mu(1-\gamma_5)$	$\gamma_\mu(1+\gamma_5)$
$\tilde{\chi}_i^0 \tilde{\chi}_1^+ W^-$	$-\frac{e}{4 sin\theta_W} \left(2 N_{i2} U_{i1} + \sqrt{2} N_{i3} U_{i2}\right)$	$-\frac{e}{4 sin\theta_W} \left(2 N_{i2} V_{i1} - \sqrt{2} N_{i4} V_{i2}\right)$
$\tilde{\chi}_i^0 \tilde{\chi}_2^+ W^-$	$-\frac{e}{4 sin\theta_W} \left(2 N_{i2} U_{i2} + \sqrt{2} N_{i3} U_{i1}\right)$	$-\frac{e}{4 sin\theta_W} \left(2 N_{i2} V_{i2} - \sqrt{2} N_{i4} V_{i1}\right)$

Tab. 3 – Neutralino couplings to chargino/W

Bibliographie

[1] W. J. G. de Blok, Stacy S. McGaugh, Albert Bosma, and Vera C. Rubin. Mass Density Profiles of LSB Galaxies. *Astrophys. J.*, 552 :L23–l26, 2001.

[2] Howard Baer and Xerxes Tata. Dark matter and the LHC. 2008.

[3] (Ed.) Kolb, Edward W. and (Ed.) Turner, Michael S. THE EARLY UNIVERSE. REPRINTS. 1988.

[4] Jonathan L. Feng. Dark Matter Candidates from Particle Physics and Methods of Detection. *Ann. Rev. Astron. Astrophys.*, 48 :495, 2010.

[5] Mark Srednicki, Richard Watkins, and Keith A. Olive. Calculations of Relic Densities in the Early Universe. *Nucl.Phys.*, B310 :693, 1988.

[6] Keith A. Olive, David N. Schramm, and Gary Steigman. Limits on New Superweakly Interacting Particles from Primordial Nucleosynthesis. *Nucl.Phys.*, B180 :497, 1981.

[7] Paolo Gondolo and Graciela Gelmini. Cosmic abundances of stable particles : Improved analysis. *Nucl.Phys.*, B360 :145–179, 1991.

[8] P. Gondolo, J. Edsjo, P. Ullio, L. Bergstrom, Mia Schelke, et al. DarkSUSY : Computing supersymmetric dark matter properties numerically. *JCAP*, 0407 :008, 2004.

[9] Howard Baer, Csaba Balazs, and Alexander Belyaev. Neutralino relic density in minimal supergravity with coannihilations. *JHEP*, 0203 :042, 2002.

[10] A. Arbey and F. Mahmoudi. SuperIso Relic v3.0 : A program for calculating relic density and flavour physics observables : Extension to NMSSM. *Comput.Phys.Commun.*, 182 :1582–1583, 2011.

[11] G. Belanger, F. Boudjema, P. Brun, A. Pukhov, S. Rosier-Lees, et al. Indirect search for dark matter with micrOMEGAs2.4. *Comput.Phys.Commun.*, 182 :842–856, 2011.

[12] Kim Griest and David Seckel. Three exceptions in the calculation of relic abundances. *Phys.Rev.*, D43 :3191–3203, 1991.

[13] D. Maurin, F. Donato, R. Taillet, and P. Salati. Cosmic rays below z=30 in a diffusion model : new constraints on propagation parameters. *Astrophys.J.*, 555 :585–596, 2001. * Brief entry *.

[14] T. Delahaye, F. Donato, N. Fornengo, J. Lavalle, R. Lineros, et al. Galactic secondary positron flux at the Earth. *Astron.Astrophys.*, 501 :821–833, 2009. * Brief entry *.

[15] O. Adriani et al. PAMELA results on the cosmic-ray antiproton flux from 60 MeV to 180 GeV in kinetic energy. *Phys.Rev.Lett.*, 105 :121101, 2010.

[16] R. Lemrani. Search for dark matter with edelweiss : Status and future. *Phys. Atom. Nucl.*, 69 :1967–1969, 2006.

[17] R. Bernabei et al. Dama investigations on dark matter at gran sasso : Results and perspectives. *AIP Conf. Proc.*, 878 :91–98, 2006.

[18] D. S. Akerib et al. Cdms, supersymmetry and extra dimensions. 2006.

[19] J. Angle et al. First results from the xenon10 dark matter experiment at the gran sasso national laboratory. 2007.

[20] F. Aubin et al. Results and status of the picasso experiment. Prepared for 9th ICATPP Conference on Astroparticle, Particle, Space Physics, Detectors and Medical Physics Applications, Villa Erba, Como, Italy, 17-21 Oct 2005.

[21] J. Lee. Kims : Dark matter search experiment in korea. *AIP Conf. Proc.*, 878 :106–110, 2006.

[22] R. Bernabei, P. Belli, F. Cappella, R. Cerulli, C.J. Dai, et al. New results from DAMA/LIBRA. *Eur.Phys.J.*, C67 :39–49, 2010. * Temporary entry *.

[23] E. Aprile et al. Dark Matter Results from 100 Live Days of XENON100 Data. *Phys.Rev.Lett.*, 2011.

[24] Toby Falk, Andrew Ferstl, and Keith A. Olive. Variations of the neutralino elastic cross-section with cp violating phases. *Astropart. Phys.*, 13 :301–316, 2000.

[25] Mikhail A. Shifman, A. I. Vainshtein, and Valentin I. Zakharov. Remarks on higgs boson interactions with nucleons. *Phys. Lett.*, B78 :443, 1978.

[26] A. Bottino, F. Donato, N. Fornengo, and S. Scopel. Size of the neutralino nucleon cross-section in the light of a new determination of the pion nucleon sigma term. *Astropart. Phys.*, 18 :205–211, 2002.

[27] J. D. Vergados. On the direct detection of dark matter : Exploring all the signatures of the neutralino nucleus interaction. 2006.

[28] John R. Ellis, Keith A. Olive, Yudi Santoso, and Vassilis C. Spanos. Update on the direct detection of supersymmetric dark matter. *Phys.Rev.*, D71 :095007, 2005.

[29] G. Belanger, F. Boudjema, A. Pukhov, and A. Semenov. Dark matter direct detection rate in a generic model with micrOMEGAs2.2. *Comput.Phys.Commun.*, 180 :747–767, 2009.

[30] Joel Giedt, Anthony W. Thomas, and Ross D. Young. Dark matter, the CMSSM and lattice QCD. *Phys.Rev.Lett.*, 103 :201802, 2009.

[31] V. A. Bednyakov and F. Simkovic. Nuclear spin structure in dark matter search : The zero momentum transfer limit. *Phys. Part. Nucl.*, 36 :131–152, 2005.

[32] Gerard Jungman, Marc Kamionkowski, and Kim Griest. Supersymmetric dark matter. *Phys.Rept.*, 267 :195–373, 1996.

[33] A. Airapetian et al. Precise determination of the spin structure function g(1) of the proton, deuteron and neutron. *Phys. Rev.*, D75 :012007, 2007.

[34] V. A. Bednyakov and F. Simkovic. Nuclear spin structure in dark matter search : The finite momentum transfer limit. *Phys. Part. Nucl.*, 37 :S106–S128, 2006.

[35] F. J. Kerr and Donald Lynden-Bell. Review of galactic constants. *Mon. Not. Roy. Astron. Soc.*, 221 :1023, 1986.

[36] Martin C. Smith et al. The rave survey : Constraining the local galactic escape speed. *Mon. Not. Roy. Astron. Soc.*, 379 :755–772, 2007.

[37] P. Belli, R. Cerulli, N. Fornengo, and S. Scopel. Effect of the galactic halo modeling on the dama/nai annual modulation result : An extended analysis of the data for wimps with a purely spin-independent coupling. *Phys. Rev.*, D66 :043503, 2002.

[38] E. Aprile et al. Implications on Inelastic Dark Matter from 100 Live Days of XENON100 Data. 2011.

[39] E. Behnke, J. Behnke, S.J. Brice, D. Broemmelsiek, J.I. Collar, et al. Improved Limits on Spin-Dependent WIMP-Proton Interactions from a Two Liter CF_3I Bubble Chamber. *Phys.Rev.Lett.*, 106 :021303, 2011.

[40] Andrew Gould. WIMP DISTRIBUTION IN AND EVAPORATION FROM THE SUN. *Astrophys.J.*, 321 :560, 1987.

[41] R. Abbasi et al. Limits on a muon flux from neutralino annihilations in the Sun with the IceCube 22-string detector. *Phys.Rev.Lett.*, 102 :201302, 2009.

[42] Marco Cirelli, Nicolao Fornengo, Teresa Montaruli, Igor A. Sokalski, Alessandro Strumia, et al. Spectra of neutrinos from dark matter annihilations. *Nucl.Phys.*, B727 :99–138, 2005.

[43] Matteo Viel. Neutrinos and the Lyman-alpha forest : Myth or reality ? *Nucl.Phys.Proc.Suppl.*, 168 :54–56, 2007.

[44] (ed.) Bertone, Gianfranco. Particle dark matter : Observations, models and searches. 2010.

[45] Pierre Sikivie. in Bertone, Gianfranco, (ed.), Particle dark matter : Observations, models and searches. 2010.

[46] Gianfranco Bertone, Dan Hooper, and Joseph Silk. Particle dark matter : Evidence, candidates and constraints. *Phys.Rept.*, 405 :279–390, 2005.

[47] John R. Ellis, Keith A. Olive, Yudi Santoso, and Vassilis C. Spanos. Supersymmetric dark matter in light of WMAP. *Phys.Lett.*, B565 :176–182, 2003.

[48] Leszek Roszkowski, Roberto Ruiz de Austri, Roberto Trotta, Yue-Lin Sming Tsai, and Tom A. Varley. Global fits of the Non-Universal Higgs Model. *Phys.Rev.*, D83 :015014, 2011.

[49] Lars Bergstrom, Joakim Edsjo, and Gabrijela Zaharijas. Dark matter interpretation of recent electron and positron data. *Phys.Rev.Lett.*, 103 :031103, 2009.